Molecular Therapy
Original Article

An SCD1-dependent mechanoresponsive pathway promotes HCC invasion and metastasis through lipid metabolic reprogramming

Hua-Hua Liu,[1,3] Yang Xu,[1,3] Cao-Jie Li,[1] Shu-Jung Hsu,[1] Xia-Hui Lin,[1] Rui Zhang,[1] Jie Chen,[1] Jun Chen,[1] Dong-Mei Gao,[1] Jie-Feng Cui,[1] Xin-Rong Yang,[1] Zheng-Gang Ren,[1,2] and Rong-Xin Chen[1,2]

[1]Liver Cancer Institute, Zhongshan Hospital, Fudan University and Key Laboratory of Carcinogenesis and Cancer Invasion, Ministry of Education, 180 Fenglin Road, Shanghai 200032, China; [2]National Clinical Research Center for Interventional Medicine, Shanghai, China

Matrix stiffness promotes hepatocellular carcinoma (HCC) metastasis. This study examined the contribution of lipid metabolic reprogramming to matrix stiffness-induced HCC metastasis. HCC cells were cultured on mechanically tunable polyacrylamide gels and subjected to lipidomic analysis. The key enzyme that responded to matrix stiffness and regulated lipid metabolism was identified. The comparative lipidomic screening revealed that stearoyl-CoA desaturase 1 (SCD1) is a mechanoresponsive enzyme that reprogrammed HCC cell lipid metabolism. The genetic and pharmacological inhibition of SCD1 expression/activity altered the cellular lipid composition, which in turn impaired plasma membrane fluidity and inhibited *in vitro* invasive motility of HCC cells in response to high matrix stiffness. Knockdown of SCD1 suppressed HCC invasion and metastasis *in vivo*. Conversely, the overexpression of SCD1 or exogenous administration of its product oleic acid augmented plasma membrane fluidity and rescued *in vitro* invasive migration in HCC cells cultured on soft substrates, mimicking the effects imposed by high matrix stiffness. In human HCC tissues, collagen content, a marker of increasing matrix stiffness, and increased expression of SCD1 together predicted poor survival of HCC patients. An SCD1-dependent mechanoresponsive pathway that responds to increasing matrix stiffness in the tumor microenvironment promotes HCC invasion and metastasis through lipid metabolic reprogramming.

INTRODUCTION

Hepatocellular carcinoma (HCC) is the third most common cause of cancer-related deaths worldwide.[1] This dismal outcome has been attributed to patients being diagnosed at late stages and the high frequency of metastasis in HCC. Even among patients with resectable HCC (most of them belonging to early stage), up to 70% will experience intra- or extra-hepatic recurrent metastasis after resection.[2] Metastasis remains the major concern that causes death in HCC patients. Elucidating the mechanism underlying HCC metastasis will provide a basis for the prevention of metastasis.[3,4]

The majority (80%) of HCC develop in liver fibrosis or cirrhosis,[5] a condition in which altered biochemical and biophysical microenvironment initiates cancer onset and progression. Matrix stiffness is a characteristic of biophysical signals in the microenvironment and potently regulates cellular behaviors in various physio-pathological processes. Abnormal matrix stiffness plays a significant role during tumor progression. Increasing matrix stiffness is a strong predictor of HCC incidence, regulates HCC cell proliferation, chemotherapeutic response,[6] invasion and metastasis,[7] and correlates with poor survival in HCC patients.[8] The signal from physical matrix stiffness is converted into various biochemical responses to drive malignant behaviors; among these, metabolic input that occurs during matrix stiffness-induced tumor progression is poorly understood.

While glycolysis accounts for rapid proliferation in cancer cells,[9] lipid metabolism not only produces more energy but also provides the raw materials for cellular components and signaling molecules for oncogenesis and metastasis.[10] Reportedly, matrix stiffness rewires metabolism in the tumors, including HCC. Matrix stiffening activates a mechano-transduction pathway of MAPK-YAP to promote aerobic glycolysis in HCC cells.[11] In addition, a matrix stiffness-dependent amino acids aspartate/glutamate exchange between stromal fibroblast and cancer cells initiates tumor progression and metastasis in squamous cell carcinoma.[12] These studies highlight the crosstalk between matrix stiffening and tumor metabolic rewiring. However, whether matrix stiffness controls lipid metabolic reprogramming to accelerate tumor progression is yet to be elucidated.

Received 26 August 2021; accepted 24 March 2022;
https://doi.org/10.1016/j.ymthe.2022.03.015.

[3]These authors contributed equally

Correspondence: Xin-Rong Yang. Liver Cancer Institute, Zhongshan Hospital, Fudan University and Key Laboratory of Carcinogenesis and Cancer Invasion, Ministry of Education, 180 Fenglin Road, Shanghai 200032, China.
E-mail: yang.xinrong@zs-hospital.sh.cn
Correspondence: Zheng-Gang Ren, National Clinical Research Center for Interventional Medicine, Shanghai, China.
E-mail: ren.zhenggang@zs-hospital.sh.cn
Correspondence: Rong-Xin Chen, National Clinical Research Center for Interventional Medicine, Shanghai, China.
E-mail: chen.rongxin@zs-hospital.sh.cn

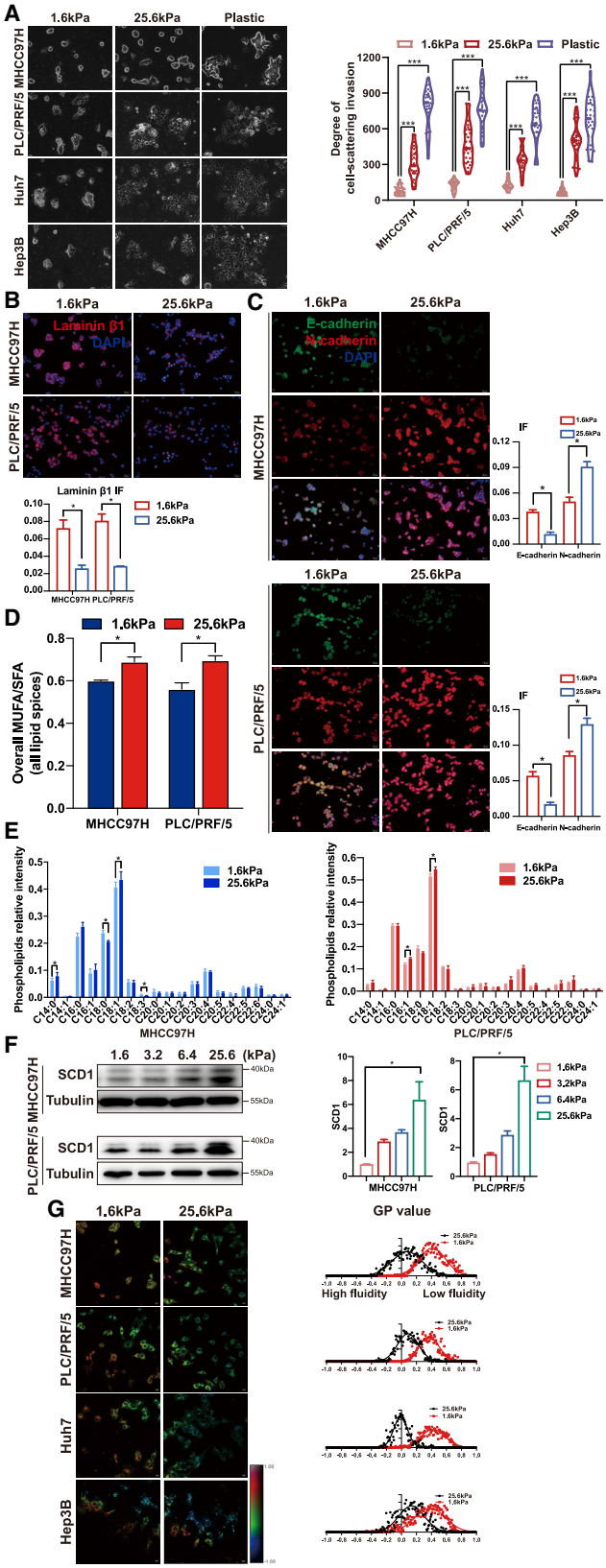

Figure 1. Matrix stiffness promotes the invasion of HCC cells

HCC cells were cultured on polyacrylamide hydrogels with the indicated rigidities (1.6 and 25.6 kPa) and plastic plates in 3D Matrigel overlay culture. (A) Bright-field images of HCC cells. The *in vitro* invasion of HCC cells is quantified by the degree of cell scattering using ImageJ software. (B and C) Expression of basement membrane component laminin β1 and EMT-related markers (E-cadherin and N-cadherin) was assessed by immunofluorescence staining. (D) Matrix stiffness modulated the ratio of monounsaturated/saturated fatty acids in all lipid species. (E) Phospholipids levels were determined by lipidomic mass spectrometry. (F) Western blot analyzed stiffness-induced SCD1 protein expression. (G) Hue-saturation-brightness images. The value of the minimum color (blue) was set to generalized polarization (GP) = −1 and the maximum (red) was set to 1. *p < 0.05, ***p < 0.001.

Previously, we found that high matrix stiffness promotes HCC metastasis.[13] Herein, we examined the specific contribution of lipid metabolic reprogramming to HCC metastasis triggered by matrix stiffness. Stearoyl-CoA desaturase 1 (SCD1) is an essential mechano-mediator that reprograms HCC cell lipid metabolism. The genetic and pharmacological modulation of SCD1 expression/activity altered the cellular lipid composition, which in turn impaired plasma membrane fluidity and inhibited invasive migration *in vitro* in HCC cells in response to matrix stiffness and reduced metastasis *in vivo*. Collagen deposit indicates increased matrix stiffness in the tumor microenvironment. In human HCC tissues, collagen content, a marker of increasing matrix stiffness, and increased expression of SCD1 together predicted poor survival in HCC patients. These findings reveal that an SCD1-dependent mechanoresponsive pathway responds to increasing matrix stiffness (the biomechanical signal in the tumor microenvironment) and promotes HCC invasion and metastasis through lipid metabolic reprogramming, thereby providing a new therapeutic target to attenuate HCC metastasis.

RESULTS

SCD1 is essential for matrix stiffness-induced lipid metabolic programming and cellular invasion

In agreement with previous observations that increasing matrix stiffness induces malignant phenotype,[14] HCC cells presented an invasive migration on stiff supports of 25.6 kPa, showing a protrusive appearance with mesenchymal phenotype and well-spread morphology in a three-dimensional (3D) Matrigel overlay culture system (Figure 1A). Since the basement membrane serves as a barrier separating epithelial cells from the surrounding stroma, the decrease in the basement membrane component laminin occurs in an early invasive stage. In Figure 1B, a pronounced decrease in the basement membrane protein laminin β1 was observed in HCC cells at 25.6 kPa, as an indicator of cellular invasion, in conjunction with changes in the epithelial marker E-cadherin and mesenchymal marker N-cadherin (Figure 1C), which highlights that increased matrix stiffness induces mesenchymal shift and cellular invasion.

To determine the contribution of lipid metabolism to matrix stiffness-induced cellular invasion, we performed a mass spectrometry-based lipidomic analysis in HCC cells plated on polyacrylamide gels with tunable matrix stiffness in a 3D Matrigel overlay culture system. A total of 1,060 unique lipids were identified through the integration of

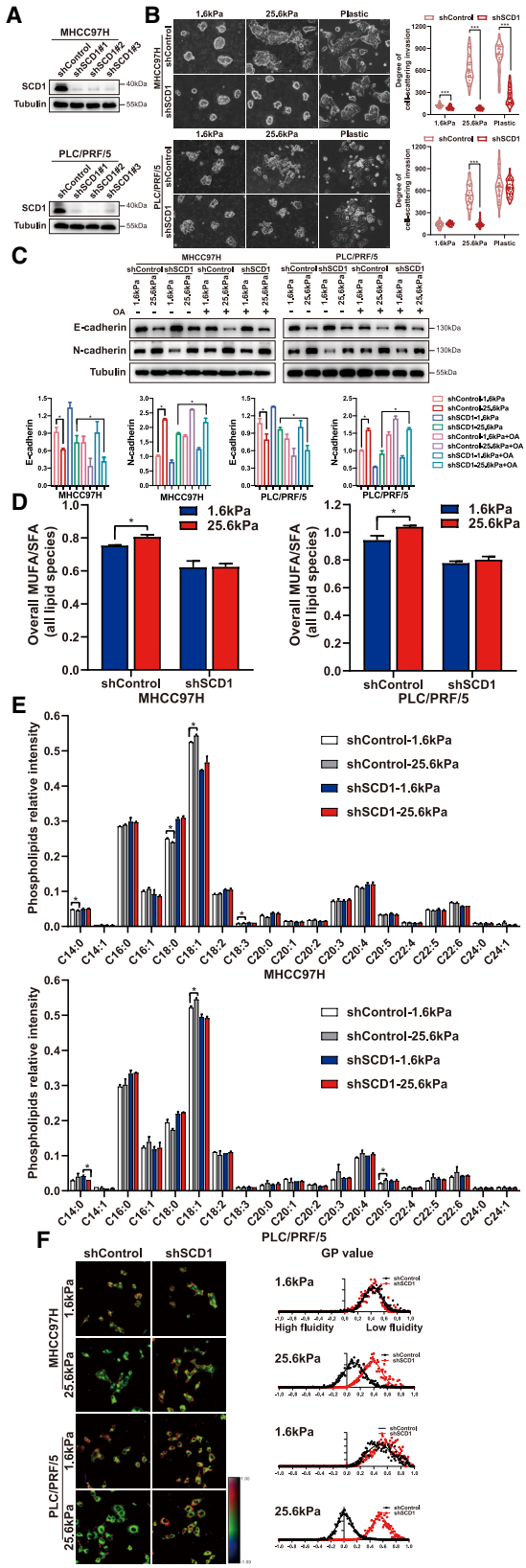

Figure 2. SCD1 is required for matrix stiffness-induced invasion in HCC cells

HCC cells expressing control (shControl) or SCD1 shRNA (shSCD1) were cultured on polyacrylamide hydrogels with the indicated rigidities (1.6 and 25.6 kPa) and plastic plates in 3D Matrigel overlay culture. (A) Efficiency of SCD1 knockdown was probed by western blot. (B) Bright-field images of HCC cells. The *in vitro* invasion of HCC cells is quantified by the degree of cell scattering using ImageJ software. (C) Expression of EMT-related markers E-cadherin and N-cadherin was assessed by western blot. HCC cells were treated with or without oleic acid (OA) (the product of SCD1). (D) Ratio of monounsaturated/saturated fatty acids in all lipid species. (E) Phospholipid levels were determined by lipidomic mass spectrometry. (F) Hue-saturation-brightness images of HCC cells. The value of the minimum color (blue) was set to generalized polarization (GP) = −1, and the maximum (red) was set to 1. *p < 0.05, ***p < 0.001.

positive and negative electrospray ionization mode, including 20 free fatty acids, 502 glycerophospholipids, 505 glycerides, 12 sphingolipids, and 21 cholesteryl esters (Figure S1A). Phosphatidylcholine and phosphatidylserine had increased trends on 25.6 kPa compared with 1.6 kPa by relative quantification (Figure S1B). A total of 125 unique lipids exhibited changes in HCC cells cultured on stiff versus soft supports; among these, 3 phosphatidic acids, 12 phosphatidylcholines, 15 phosphatidylethanolamines, 4 phosphatidylglycerols, 10 phosphatidylinositols, and 12 phosphatidylserines were significantly increased (Figures S1C and S2). First, we noted that the ratio of monounsaturated fatty acid/saturated fatty acid (MUFA/SFA) was increased across most lipid classes (Figure 1D). Among these lipids, membrane phospholipids containing the C18:1 unsaturated fatty acid was predominantly increased in MHCC97H and PLC/PRF/5 (Figure 1E), with a significant increase of C16:1 fatty acyl chain in PLC/PRF/5. Meanwhile, membrane phospholipids containing C18:0 were significantly decreased in MHCC97H and showed a non-significant decreasing trend in PLC/PRF/5. These findings suggest that SCD1 might be responsible for matrix stiffness-induced lipid reprogramming because SCD1 is a rate-limiting enzyme in monounsaturated fatty acid synthesis. The protein levels of SCD1 increased proportionally to stiffness (Figure 1F). The membrane content phospholipids affect the invasion of cancer cells by modulating plasma membrane fluidity; higher plasma membrane fluidity was detected in HCC cells cultured on stiff versus soft supports, which was measured by a biophysical parameter-generalized polarization (GP) value inversely correlated with membrane fluidity (MHCC97H, 0.07 versus 0.41; PLC/PRF/5 0.09 versus 0.36, Huh7 -0.01 versus 0.42; Hep3B 0.13 versus 0.38; all $p < 0.05$) (Figure 1G). These phenomena indicate that SCD1 might be involved in matrix stiffness-trigged lipid metabolic reprogramming, which in turn influences membrane fluidity and cellular invasion.

Next, we investigated whether SCD1 is required for matrix stiffness-induced lipid metabolic reprogramming and cellular invasion. We generated HCC cells expressing short hairpin RNAs (shRNA) against SCD1 and tested the impact of SCD1 on the mechanoresponsive pathway. The knockdown of SCD1 significantly attenuated the HCC cell-invasive phenotype at high matrix stiffness; these cells were round with decreased N-cadherin and increased E-cadherin on rigid matrix substrates (Figures 2A–2C). These data demonstrate

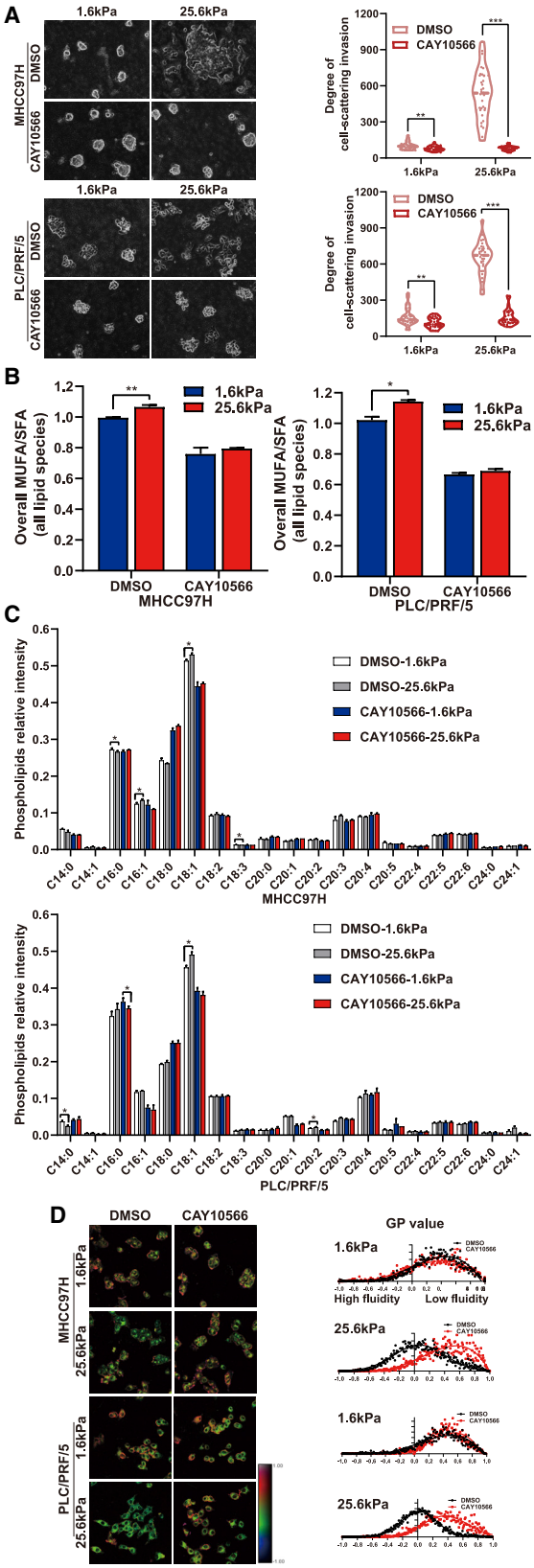

Figure 3. Pharmacological disruption of SCD1 activity suppresses matrix stiffness-induced invasion in HCC cells

HCC cells were cultured on polyacrylamide hydrogels with the indicated rigidities (1.6 and 25.6 kPa) in 3D Matrigel overlay culture and treated with DMSO or SCD1 inhibitor CAY10566. (A) Bright-field images of HCC cells. The *in vitro* invasion of HCC cells is quantified by the degree of cell scattering using ImageJ software. (B) Ratio of monounsaturated/saturated fatty acid in all lipid species. (C) Phospholipids levels were determined by lipidomic mass spectrometry. (D) Hue-saturation-brightness images of HCC cells. The value of the minimum color (blue) was set to generalized polarization (GP) = −1, and the maximum (red) was set to 1. *p < 0.05, **p < 0.01, ***p < 0.001.

that high matrix stiffness-induced HCC cell invasion is SCD1 dependent. Importantly, the knockdown of SCD1 reversed lipid metabolism reprogramming induced by high matrix stiffness, as displayed by the notably reduced MUFA/SFA ratio and membrane phospholipids containing the C18:1 fatty acyl chain (Figures 2D and 2E). This led to a significant blocking of membrane fluidity of HCC cells on high matrix stiffness at 25.6 kPa (GP value, MHCC97H, 0.38 versus 0.11; PLC/PRF/5, 0.55 versus 0.11; $p < 0.05$) (Figure 2F). The pharmacological disruption of SCD1 activity using SCD1 inhibitor CAY10566 significantly tempered matrix stiffness-mediated regulation of cellular invasion, lipid metabolism reprogramming, and plasma membrane fluidity in HCC cells cultured on stiff supports (Figures 3A–3D). These data indicate an essential role for SCD1 in mediating the response of HCC cells to a matrix stiffness-driven lipid metabolic reprogramming and pro-invasive cue.

To further characterize the critical function of SCD1 during matrix stiffness-induced cellular invasion, SCD1 was overexpressed in HCC cells. Remarkably, the upregulation of SCD1 induced cell spreading or rescued cellular invasion of HCC cells on the soft supports (Figures 4A and 4B) with increased N-cadherin and reduced E-cadherin levels (Figure 4C). The altered lipid metabolism was observed with respect to increased MUFA/SFA ratio and membrane phospholipids containing the C18:1 fatty acyl chain, and increased plasma membrane fluidity was detected in SCD1-overexpressing HCC cells cultured on soft substrates (MHCC97H, 0.03 versus 0.35; PLC/PRF/5, 0.04 versus 0.39; all $p < 0.05$) (Figures 4D–4F). However, the overexpression of SCD1 did not show any statistically significant increase in the plasma membrane fluidity of HCC cells at 25.6 kPa (Figure 4F), implying that SCD1 product stimulated by high matrix stiffness is sufficient to maintain membrane fluidity for an invasive phenotype. These results suggested that SCD1 overexpression and its downstream regulators rescue the invasive motility of HCC cells on the soft supports, thereby mimicking the effects imposed by stiff supports.

Taken together, the above data strongly support SCD1 as a mechanoresponsive target mediating matrix stiffness-induced lipid programming and cellular invasion in HCC cells.

SCD1 is upregulated by high matrix stiffness

To determine whether SCD1-mediated protrusive invasion in HCC cells could be reversed if high-stiffness matrices returned to a low level, we first cultured HCC cells on either high- or low-stiffness matrices until the pattern of invasive migration was clear and then

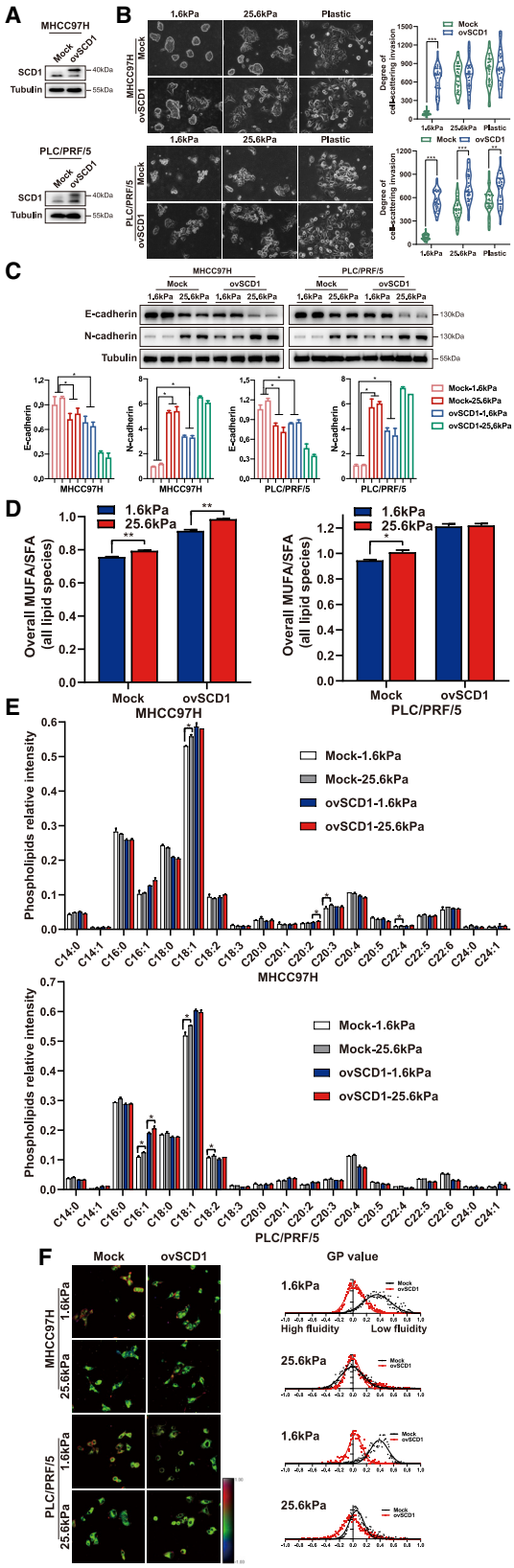

Figure 4. Upregulation of SCD1 expression rescues the invasion of HCC cells cultured on soft matrix substrates

HCC cells transfected with mock or SCD1-expressing plasmid (ovSCD1) were cultured on polyacrylamide hydrogels with the indicated rigidities (1.6 and 25.6 kPa) and plastic plates in 3D Matrigel overlay culture. (A) SCD1 protein expression was analyzed by western blot. (B) Bright-field images of HCC cells. The *in vitro* invasion of HCC cells was quantified by the degree of cell scattering using ImageJ software. (C) The expression of EMT-related markers (E-cadherin and N-cadherin) was assessed by western blot. (D) Ratio of monounsaturated/saturated fatty acids in all lipid species. (E) Phospholipids levels were determined by lipidomic mass spectrometry. (F) Hue-saturation-brightness images of HCC cells. The value of the minimum color (blue) was set to generalized polarization (GP) = −1 and the maximum (red) was set to 1. *p < 0.05, **p < 0.01, ***p < 0.001.

transferred the HCC cells to another matrix stiffness environment. The transfer from low- to high-stiffness matrices raised the level of SCD1 and protrusive migration in the new stiffness environment, whereas the transfer from high to low matrices resulted in an SCD1 decrease and a retraction of protrusions and confined growth (Figures 5A and 5B). However, these invasive phenotypic transitions were lost in SCD1 knockdown cells (Figure 5A). These results suggest that the local matrix stiffness environment determines the SCD1-mediated invasive migration strategy in HCC cells.

As described above, SCD1 protein expression was elevated in HCC cells on stiff versus soft matrix (Figure 1F), whereas its mRNA expression under different matrix rigidities did not differ significantly (Figure 5C). Surprisingly, in the presence of a protein synthesis inhibitor, cycloheximide, SCD1 protein in HCC cells on the soft matrix degraded faster than that on the stiff matrix (Figure 5D). Moreover, treatment with a proteasome inhibitor MG-132 increased the expression of SCD1 protein in HCC cells (Figure 5E). To determine whether stiffness could influence the ubiquitination status of SCD1 and thus promote its degradation, ubiquitination analyses were performed under different matrix rigidities. The ubiquitination level of SCD1 was markedly increased in HCC cells cultured on the soft versus stiff matrix (Figure 5F). Therefore, the SCD1 protein underwent accelerated proteasomal degradation in HCC cells on soft substrates, whereas it was more stabilized in cells cultured on stiff matrices.

To determine the pathway associated with SCD1 upregulation by matrix stiffness, we utilized a function-blocking anti-β1-integrin antibody and pharmacological FAK inhibitor PF562271. The anti-β1-integrin antibody and PF562271 reversed the high matrix stiffness-mediated upregulation of SCD1 (Figures 5G and 5H).

Together, these results indicate that high matrix stiffness-mediated SCD1 increase occurs through integrin β1/FAK signaling pathway activation and downregulation of SCD1 ubiquitin-proteasomal degradation.

Oleic acid, the product of SCD1, reverses SCD1 knockdown-mediated inhibition of cellular invasion

SCD1 catalyzes *de novo* synthesis of monounsaturated fatty acids from saturated fatty acids, especially stearic acid (18:0) and palmitic

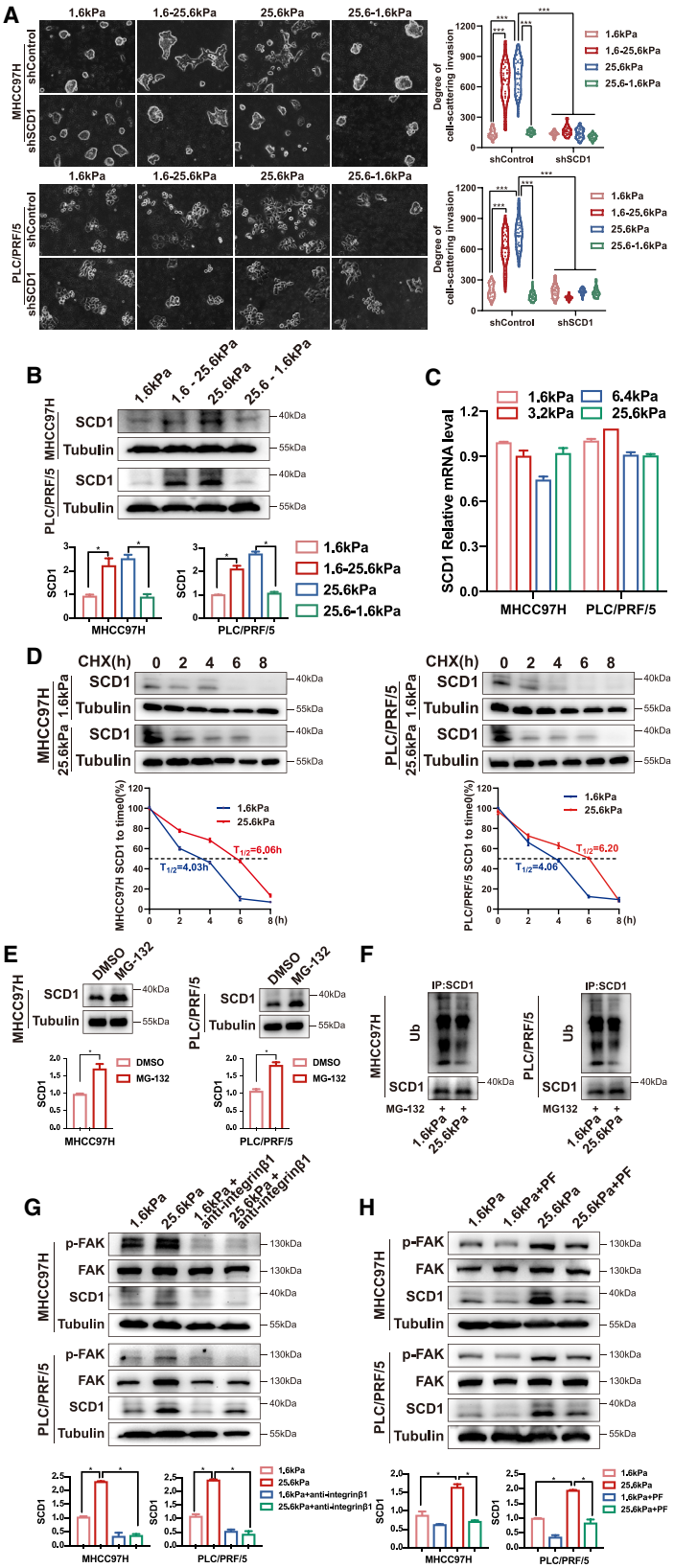

Figure 5. Matrix stiffness modulates SCD1 expression

HCC cells expressing control (shControl) or SCD1 shRNA (shSCD1) were grown on polyacrylamide hydrogels with the indicated rigidities (1.6 and 25.6 kPa) and then switched from 1.6 to 25.6 kPa (1.6–25.6 kPa) or from 25.6 to 1.6 kPa (25.6–1.6 kPa) in 3D Matrigel overlay culture (A) Representative bright-field images of HCC cells. The *in vitro* invasion of HCC cells is quantified by the degree of cell scattering using ImageJ software. (B) SCD1 expression was analyzed by western blot. (C) qRT-PCR analysis of SCD1 mRNA expression in HCC cells on polyacrylamide hydrogels with the indicated rigidities (1.6, 3.2, 6.4, and 25.6 kPa) in 3D Matrigel overlay culture. (D) Effect of matrix stiffness on SCD1 protein stability was analyzed by western blot in the presence of cycloheximide (CHX). The half-life (T1/2) of SCD1 was calculated. HCC cells were collected at the indicated time points after exposure to CHX, and cell lysates were subjected to immunoblotting. (E) SCD1 protein expression was increased in HCC cells treated with the proteasome inhibitor MG-132. (F) The level of ubiquitinated SCD1 was reduced in HCC cells cultured on stiff matrix. (G and H) HCC cells were treated with the anti-β1-integrin antibody or p-FAK inhibitor PF562271 (PF). SCD1 expression was analyzed by western blot. ***$p < 0.001$.

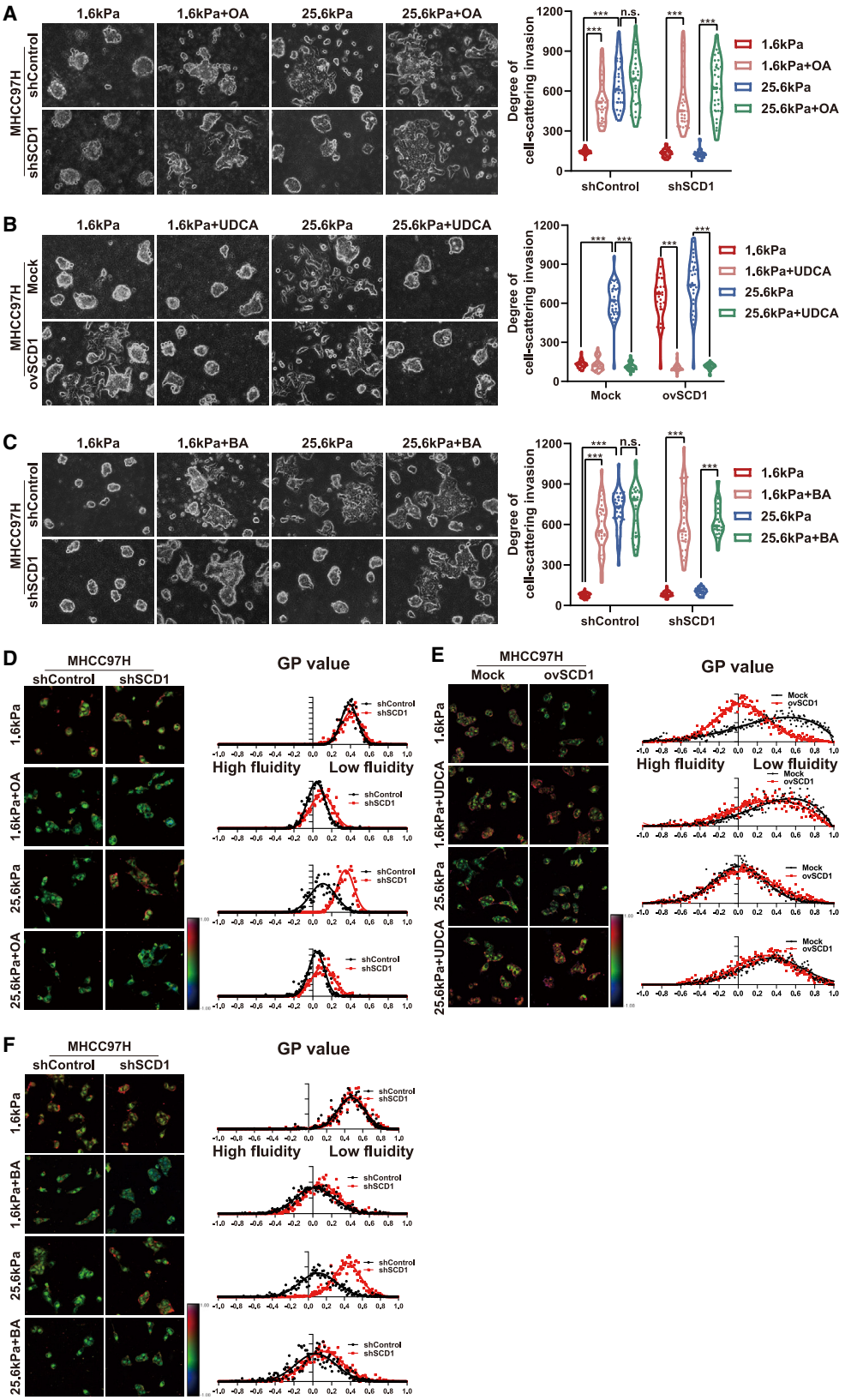

(legend on next page)

acid (16:0) to their Δ9-*cis* monounsaturated oleic acid (OA) (18:1) and palmitoleic acid (16:1).[15] As described above, knockdown of SCD1 inhibited matrix stiffness-induced cellular invasion in HCC cells by reduced membrane phospholipids containing the C18:1 fatty acyl chain (Figures 2B and 2E). Next, we evaluated the impact of the main lipid product of SCD1, OA, on the matrix stiffness-induced lipid metabolic reprogramming, plasma membrane fluidity, and cellular invasion. The HCC cells were incubated with a non-cytotoxic concentration (100 μM) of OA, and then membrane fluidity and invasive cellular motility were analyzed. The supplementation of OA reversed the SCD1 knockdown-mediated E-cadherin increase and N-cadherin decrease in HCC cells on the stiff supports (Figure 2C). The addition of OA significantly increased the basal membrane fluidity and invasive motility in HCC cells on the soft matrices. Notably, OA significantly reversed the SCD1 knockdown-mediated inhibition of membrane fluidity and invasive migration of HCC cells on stiff supports (Figures 6A, 6D, S3A, and S3D). These results indicate that OA is an effector in matrix stiffness-SCD1-mediated membrane fluidity and cellular invasion.

Increased membrane fluidity mediates matrix stiffness-induced cellular invasion

Membrane fluidization promotes the invasion of cancer cells. As described above, increased matrix stiffness promotes plasma membrane fluidity. To determine the role of membrane fluidity in matrix stiffness-induced cellular invasion, HCC cells were pretreated with the membrane-stabilizing agent ursodeoxycholic acid (UDCA) or the compound benzyl alcohol (BA) that fluidifies plasma membranes. Pre-incubation of HCC cells with UDCA significantly attenuated the high matrix stiffness-mediated increase in membrane fluidity and invasive motility (Figures 6B, 6E, S3B, and S3E). Conversely, BA treatment significantly enhanced cell membrane fluidity in HCC cells on soft supports, leading to the cells acquiring invasive migration (Figures 6C, 6F, S3C, and S3F). More importantly, UDCA significantly abrogated the SCD1 overexpressing increased membrane fluidity and invasive motility in HCC cells on soft supports (Figures 6B, 6E, S3B, and S3E). Concurrently, BA treatment reversed the SCD1-knockdown inhibition of membrane fluidity and invasive motility in HCC cells on stiff supports (Figures 6C, 6F, S3C, and S3F). Collectively, these data indicate a pivotal function of membrane fluidity in the matrix stiffness-SCD1 axis-induced cell-invasive motility.

Knockdown of SCD1 suppressed HCC invasion and metastasis *in vivo*

To investigate the role of SCD1 in HCC progression *in vivo*, we employed a metastatic MHCC97H HCC xenograft model, which recapitulates the metastasis of human HCC.[4] The knockdown of SCD1 significantly attenuated an invasive phenotype in MHCC97H cells cultured on high matrix stiffness in a 3D Matrigel culture system (Figure 2B), indicating that the SCD1 mechanoresponsive pathway is intact in these HCC cells. Mice were subcutaneously injected with a cell suspension of MHCC97H^{shSCD1}or MHCC97H^{shControl} cells. As shown in Figure 7A, the growth rate of tumors derived from MHCC97H^{shSCD1} cells was significantly slower than that of control tumors. Similarly, the weight of tumors in MHCC97H^{shSCD1}group was significantly reduced compared with the control group (Figure 7B), suggesting that SCD1 promotes tumor growth and progression. In the tumors from the MHCC97H^{shSCD1} group, SCD1, Ki-67, N-cadherin, and α-SMA expression was significantly decreased, whereas that of E-cadherin was markedly increased (Figure 7C). To further define the role of SCD1 in HCC metastasis, we orthotopically implanted the subcutaneous tumors into the livers of nude mice and allowed tumor development for 7 weeks. Consistent with the results of subcutaneous tumors, the volume and weight of liver tumors *in situ* in MHCC97H^{shSCD1} group were reduced than those in the control group (Figure 7D). Importantly, MHCC97H^{shSCD1} tumors presented a nested architecture characterized by a less-invasive tumor edge and a significant decrease in the number of distant lung metastases compared with the control tumors (Figure 7E). Together, these results support a critical role of SCD1 in modulating HCC invasion and metastasis *in vivo*.

Increased collagen content and SCD1 upregulation synergistically predict poor outcome in HCC patients

Next, we investigated whether the SCD1 mechanoresponsive pathway had a significant role in human HCC progression. SCD1 protein was highly expressed in tumor tissues compared with paired non-tumoral tissues in 12 HCC patients (Figure 8A). SCD1 expression and intratumoral collagen content were determined in the tissue microarrays from a cohort of 110 HCC patients. The clinicopathologic characteristics of patients are summarized in Table S1. SCD1 protein expression was restricted to the HCC cells (Figure 8B). As a surrogate marker for tissue rigidity, collagen content determined by Masson trichrome staining was automatically quantified using Image Pro Plus 6.0 software. The collagen content was significantly

Figure 6. Membrane fluidity mediates matrix stiffness-induced cellular invasion in HCC cells

(A) MHCC97H cells expressing control (shControl) or SCD1 shRNA (shSCD1) were grown on polyacrylamide hydrogels with the indicated rigidities (1.6 and 25.6 kPa) in the presence of oleic acid (OA) in 3D Matrigel overlay culture. (B) MHCC97H cells were transfected with mock or SCD1-expressing plasmid (ovSCD1) and cultured on polyacrylamide hydrogels with the indicated rigidities (1.6 and 25.6 kPa) in 3D Matrigel overlay culture and then treated with membrane-stabilizing agent UDCA. (C) MHCC97H cells expressing control (shControl) or SCD1 shRNA (shSCD1) were cultured on polyacrylamide hydrogels with the indicated rigidities (1.6 and 25.6 kPa) in 3D Matrigel overlay culture and treated with membrane-agonist compound BA. The *in vitro* invasion of HCC cells was quantified by the degree of cell scattering using ImageJ software and GraphPad Prism 8. (D) Hue-saturation-brightness images of MHCC97H cells expressing shControl or shSCD1 in the presence of OA. (E) Hue-saturation-brightness images of MHCC97H cells transfected with mock or ovSCD1 treated with/without UDCA. (F) Hue-saturation-brightness images of MHCC97H cells expressing shControl or shSCD1 treated with/without compound BA. ***$p < 0.001$.

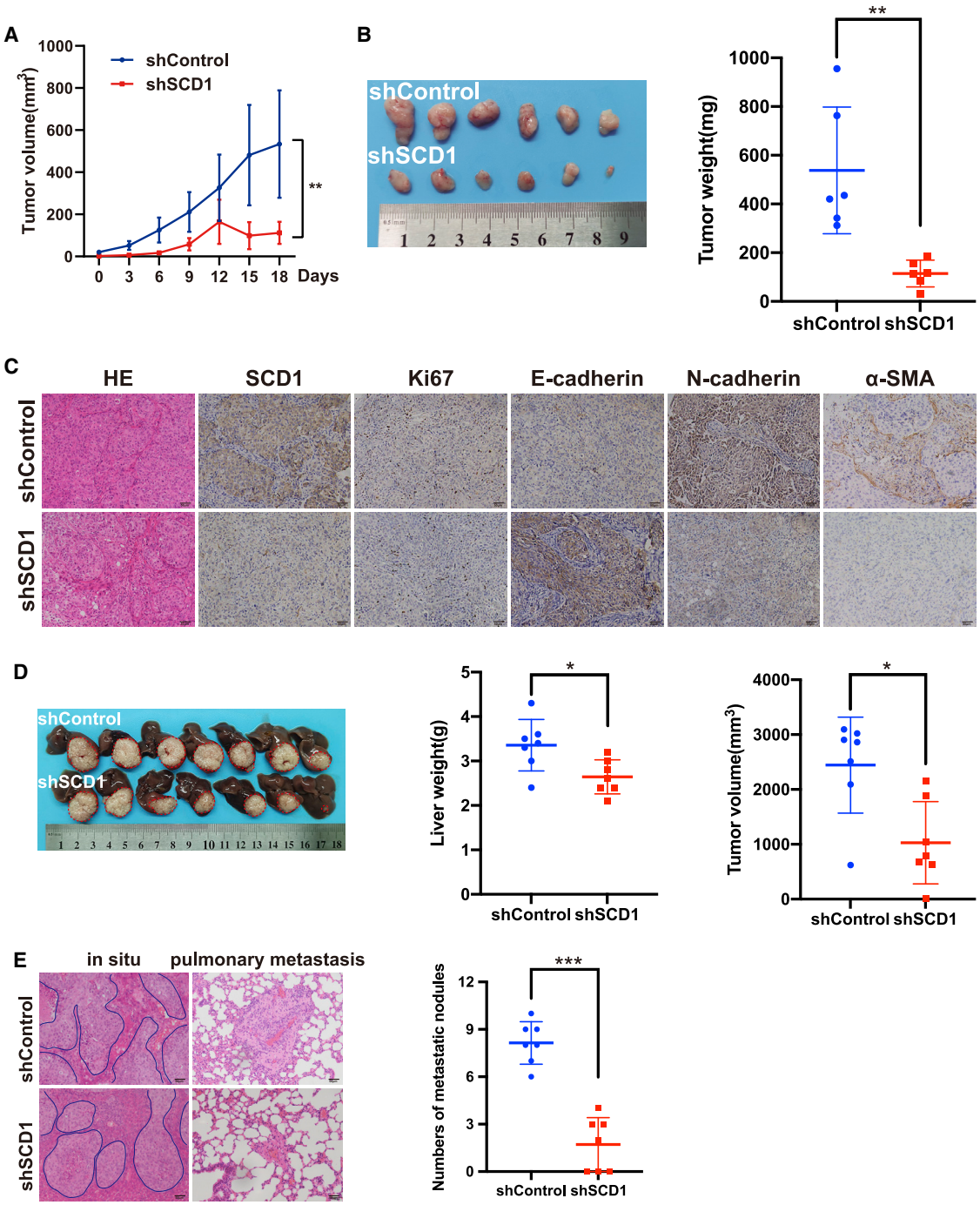

Figure 7. Knockdown of SCD1 suppresses HCC invasion and metastasis *in vivo*

(A) The growth curve of subcutaneous tumors derived from SCD1 knockdown or control MHCC97H cells (shSCD1 versus shControl) in nude mice. (B) Weight of subcutaneous tumors from SCD1 knockdown or control MHCC97H cells (shSCD1 versus shControl). (C) Expression of SCD1, α-SMA, Ki67, and EMT-related markers (E-cadherin and N-cadherin) was analyzed by immunohistochemistry. (D) Subcutaneous tumors were orthotopically implanted into the livers of nude mice and allowed tumor development. (E) *In situ* liver tumors derived from SCD1 knockdown versus shControl MHCC97H cells presented a less invasive tumor edge and a decrease in the number of distant lung metastases, as indicated by H&E staining. $^{**}p < 0.01$, $^{***}p < 0.001$.

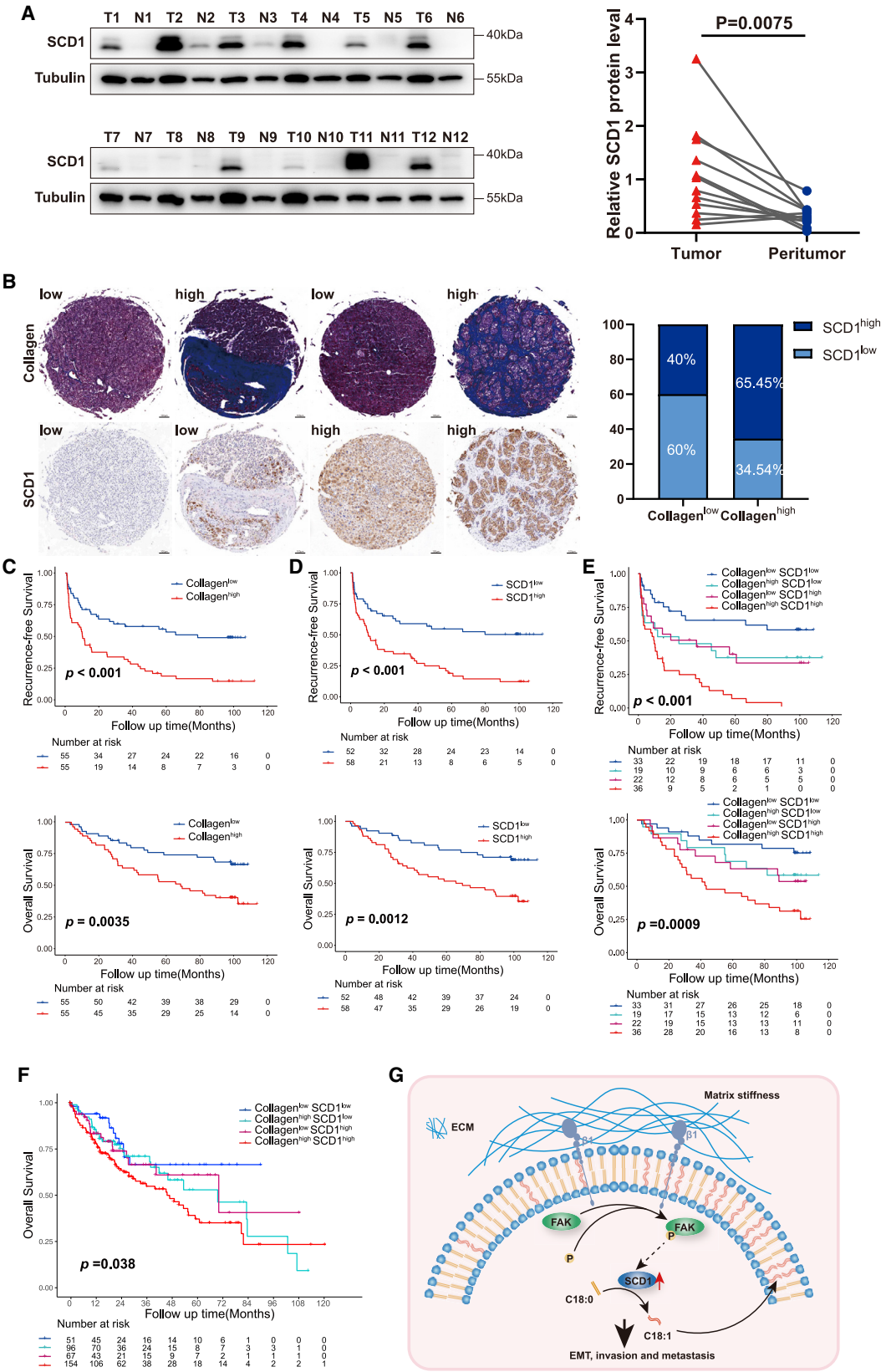

(legend on next page)

correlated with the level of SCD1 expression in HCC (Figure 8B). The patients with stiffer tumors (high collagen content $\geq$11.98%) had a poor 5-year recurrence-free survival (RFS) and overall survival (OS) of 16.90% and 52.73% compared with 54.70% and 74.06% in patients with compliant tumors (low collagen content <11.98%) ($p < 0.01$; Figure 8C), respectively. The patients with high SCD1 expression had more unfavorable outcome than those with low SCD1 expression (5-year RFS: 18.20% versus 54.32%; 5-year OS: 51.40% versus 76.70%) ($p < 0.01$; Figure 8D). Importantly, the level of SCD1 expression, together with collagen content, indicated that matrix stiffness stratified HCC patient prognosis. Patients with collagen^{high}/SCD1^{high} tumors had markedly poor outcomes with a 5-year RFS and OS of 6.02% and 44.44% compared with 65.00% and 81.50% in patients with collagen^{low}/SCD1^{low} tumors ($p < 0.001$, Figure 8E). Furthermore, patients with tumors presented as either collagen^{high} or SCD1^{high} had intermediate survival outcomes (5-year RFS: 36.80% and 39.40%; 5-year OS: 68.40% and 62.80%, respectively; Figure 8E). These indicated the cooperative effect of increasing matrix stiffness and SCD1 upregulation on HCC progression. Similar to the importance of tumor size, the association between collagen^{high}/SCD1^{high} tumors and poor prognosis was independent of other clinicopathological parameters, including gender, and Child-Pugh and BCLC staging (Tables S2 and S3). In addition, collagen^{high}/SCD1^{high} tumors predicted poor survival in The Cancer Genome Atlas-HCC cohort (Figure 8F). Thus, these findings indicate that increasing matrix stiffness in the HCC tumor microenvironment in concert with SCD1 upregulation promotes HCC recurrence and progression, and predicts poor prognosis.

DISCUSSION

Matrix stiffness is a physical cue in the tumor environment that significantly increases carcinogenesis and tumor progression.[16,17] To the best of our knowledge, this is the first study that reveals that the SCD1-mediated mechanoresponsive pathway is upregulated by high matrix stiffness. This leads to lipid metabolic reprogramming and increased plasma membrane fluidity, which in turn promotes HCC cell-invasive migration and metastasis. This study provided a new potential approach by decreasing SCD1 expression/activity to reduce matrix stiffness-induced HCC metastatic dissemination.

HCC frequently develops and progresses in the fibrotic or cirrhotic liver with increased matrix rigidity, which has led to detrimental interactions between the altered biomechanical environment and HCC.[18] Moreover, most of the HCC lesions are stiffer than their surrounding liver tissues.[19] The increase in extra-/intratumoral tissue rigidity or matrix stiffness plays a significant role in HCC progression.[20,21] Reportedly, the mechanical forces derived from matrix stiffness underlie the physio-pathological processes, including development,[22] inflammation,[23] and cancer.[24–26] For example, stem cells differentiate into specific lineages in response to various matrix elasticities;[27] mammary epithelial cells grown on the matrix with rigidity similar to the stiffness of breast cancer exhibit EMT-morphological features and invade into the basement membrane.[7] The physical signal derived from matrix stiffness is a characteristic feature in the mechanical properties of extracellular matrix and transformed into intracellular biochemical responses to direct cancer cell behavior.[28–30] However, metabolic input during matrix stiffness-induced tumor metastasis is largely unknown. Only a few studies have yet addressed the interconnection between matrix stiffening and tumor metabolic rewiring in cancer. This study explored the direct connection between matrix stiffness and lipid metabolic reprogramming. We used lipidomic analysis and identified changes in the lipid composition in HCC cells in response to matrix stiffness. Moreover, SCD1 was identified as an unanticipated target enzyme modulated by matrix stiffness. Lipid metabolic reprogramming initiated by matrix stiffness was orchestrated in an SCD1-dependent mechanoresponsive manner.

In this study, we showed that the expression level and activity of SCD1 affected the matrix stiffness-induced MUFA/SFA ratio and the lipid metabolism in HCC cells. An increase in matrix stiffness-induced fatty acid desaturation was reversed by SCD1 inhibition. Membrane fluidity alteration has been described in various pathologies, including cancer, which is regulated by modification of MUFA/SFA ratio. The type of fatty acids in the structure of the cell membrane can influence its fluidity, which is closely related to the fatty acyl chain saturation of phospholipid molecules.[31] Saturated fatty acids with a straight, rigid chain form an ordered structure and the phospholipids form a rigid bilayer; hence, the fluidity of membranes formed by saturated fatty acids is low, while membranes formed by *cis*-unsaturated fatty acids are flexible. Among these lipids in membranes, phospholipids play a critical role in the structural components of membranes on cell growth, differentiation, and motility.[32] As components in the two-layered sheets of lipid molecules, phospholipids with a C18:1 monounsaturated fatty acyl chain can induce membrane curvature,[33] which may account for the increased membrane fluidity in response to elevated matrix stiffness in this study. In addition, SCD1 inhibition antagonized the effects of high matrix stiffness on membrane fluidity,

Figure 8. Increased collagen content and SCD1 upregulation synergistically predict poor prognosis in HCC patients

(A) SCD1 protein expression in the tumor and non-tumoral tissues detected by western blot. T, tumor tissues; N, non-tumoral tissues. (B) Representative images of HCC tissues analyzed for intratumoral collagen content by Masson's trichrome staining and SCD1 expression by immunohistochemistry staining. Correlation analysis between intratumoral collagen content and SCD1 expression. (C and D) Kaplan-Meier curve of recurrence-free survival and OS for HCC patients stratified by intratumoral collagen content or SCD1 expression. (E) Kaplan-Meier curve of recurrence-free survival and OS for HCC patients stratified by intratumoral collagen content and SCD1 expression (collagen^{high}/SCD1^{high} versus collagen^{high}/SCD1^{low} versus collagen^{low}/SCD1^{high} versus collagen^{low}/SCD1^{low} tumors). (F) Kaplan-Meier curve of OS for HCC patients stratified by collagen content and SCD1 expression in The Cancer Genome Atlas-HCC cohort. (G) Schematic of the proposed mechanism that an SCD1-dependent mechanoresponsive pathway responsive to increasing matrix stiffness promotes HCC invasion and metastasis through lipid metabolic reprogramming. ECM, extracellular matrix; β1, integrin β1; FAK, focal adhesion kinase; EMT, epithelial mesenchymal transformation.

a prominent feature of cancer cell invasion. SCD1 knockdown-mediated inhibition of membrane fluidization and cell invasion is reversed by pre-incubation with exogenous OA, one of the SCD1 product. Also, a perturbation of membrane fluidity by membrane-stabilizing agent ameliorates a direct action of high matrix stiffness on cellular invasion. Furthermore, SCD1 overexpression led to an increase in fatty acid desaturation and rescued the invasive motility of HCC cells cultured on soft supports. SCD1 knockdown inhibited HCC metastasis *in vivo*. Taken together, we propose a new mechanism in which a matrix stiffness-SCD1 axis regulates lipid metabolism to promote HCC invasion and metastasis, thereby suggesting that SCD1 is a novel therapeutic target to reduce matrix stiffness-induced HCC metastasis.

In this study, we show that the pro-invasive activity conferred by matrix stiffness is through SCD1-mediated fatty acid desaturation, providing a basis for evaluating an SCD1 target for inhibiting HCC metastasis. SCD1 inhibition will reduce fatty acid desaturation, modify a pathological interaction between matrix stiffness and lipid metabolism, and decrease membrane fluidity, thus alleviating matrix stiffness-induced cellular invasion. An important feature of cancer cells is the enrichment of unsaturated fatty acids in lipid composition to form various cell membranes, supporting tumorigenesis and malignant progression.[34] SCD family converting saturated fatty acids to Δ9-monounsaturated fatty acids is correlated with cancer aggressiveness and poor outcomes of patients.[35] Studies have shown that SCD1 is involved in the biological behaviors of cancer cell proliferation, migration, metastasis, and maintaining cancer stem cell characteristics of cancer stem cells,[36] implicating that it is a promising target for anticancer therapy. SCD1 inhibitors for the treatment of cancer have been developed and preclinically tested. Currently, there are two SCD isoforms in humans, SCD1 and SCD5,[37] that contribute to fatty acid desaturation and exert a high activity on C16 or C18 substrates. Since SCD1 is ubiquitously expressed in various tissues, including the liver, there are potential off-target side effects of SCD inhibition. Surprisingly, SCD1 inhibitors have shown a favorable tolerance in clinical studies.[38]

Collagen deposition is a surrogate marker for increasing matrix stiffness in the tumor microenvironment and is associated with tumor progression.[39] In this study, collagen content, together with increased expression of SCD1, predicted the elevated risk of metastatic relapse in a relatively large cohort of HCC patients, thereby indicating that increased matrix stiffness in the tumor microenvironment leads to SCD1 upregulation that promotes HCC recurrence and metastasis.

Nevertheless, this study has some limitations. Firstly, the direct molecular mechanism by which matrix stiffness fine-tuned SCD1 expression is not determined. Although our data indicate that high matrix stiffness promotes SCD1 expression through activated integrin β1/FAK signaling and decreased SCD1 proteasomal degradation, how the FAK pathway affects the ubiquitination of SCD1 has not been dissected in this study. Also, the ubiquitination pathway that mediates SCD1 ubiquitination and then affects its protein expression level is not clarified. Moreover, how OA (the main product of SCD1) modulates the downstream targets has not been resolved. Secondly, we used pharmacological and genetic approaches and showed that the level of SCD1 expression affected matrix stiffness-triggered EMT. How SCD1 triggered EMT is not clarified in this study. One study reported that a metabolic acyl-CoA synthetase (ACSL)/SCD pathway causes EMT, which promotes migration and invasion of colon cancer cells.[40] Another study showed that hyperglycemia induces EMT in colorectal cancer cells via the SCD1-MUFA axis and by suppressing PTEN.[41] Thus, it will be interesting to explore whether the matrix stiffness-SCD1 axis induces EMT in HCC cells through the same or different mechanism.

In conclusion (Figure 8G), this study provides a new mechanistic linking matrix stiffness-SCD1 axis to lipid metabolic reprogramming and HCC metastasis, indicating that the SCD1-dependent mechanoresponsive pathway is a potential therapeutic target for anti-HCC metastasis.

MATERIALS AND METHODS

Quantification of membrane fluidity

Plasma membrane fluidity was quantified by the laser scanning platform as described previously.[41,42] Living cells were labeled with polarity-sensitive membrane probe laurdan (6-dodecanoyl-2-dimethylamino-napthalene) (Aladdin, China), which provides information about membrane fluidity by the shift in the emission spectrum. The laurdan intensity images were obtained under excitation at 405 nm, and fluorescence emission was recorded simultaneously through two channels of 400–460 and 470–530 nm. Cell membrane fluidity was expressed in the form of pseudo-colored GP values by ImageJ software (National Institutes of Health, Bethesda, MD, USA). The GP values were calculated using the formula: $GP = (I_{400\text{-}460} - GI_{470\text{-}530})/(I_{400\text{-}460} + GI_{470\text{-}530})$ where G (the calibration factor) was obtained for laurdan in dimethyl sulfoxide (DMSO) (Sigma) and I indicated the intensity of pixels in the images acquired in specified channels. The GP value was calculated in multiple regions of the cell membrane (n = 10) per group, which is inversely correlated with membrane fluidity.

HCC tissues

This study was approved by the Zhongshan Hospital of Fudan University Research Ethics Committee, and written informed consent was obtained from each patient. HCC and matched non-tumoral liver tissues from 12 patients who underwent curative liver resection and did not receive preoperative therapy were collected from Zhongshan Hospital of Fudan University from July 2015 to August 2017. A total of 110 HCC specimens collected between August 2010 and June 2011 were used for tumor tissue microarrays (TMAs). Duplicated tissue cores of 1-mm diameter were obtained from the same tissue block. The TMAs were constructed as described previously[43] and stained for SCD1 for retrospective analysis. The TMAs were also stained with Masson's trichrome to evaluate the degree of collagen deposition. SCD1 staining was scored blindly by two investigators according to the following criteria: 0 for no expression, 1+ for very weak expression, 2+ for moderate expression in >75% of tumor cells, and 3+ for

strong expression in >75% of tumor cells. The collagen content in tumors was quantified in the images with five random fields per tumor using the ImageJ method as described previously.[44]

In vivo study

All animal experiments were approved by the Committee on Animal Research of Zhongshan Hospital (Shanghai, China) and performed in accordance with the guidelines formulated by Shanghai Medical Experimental Animal Care Commission.

A metastatic model of human HCC in nude mice using MHCC97H cells was established as described previously.[45] In brief, 5×10^6 HCC cells ($MHCC97H^{shSCD1}$or $MHCC97H^{shControl}$) suspended in PBS were injected into the upper left flank region of BALB/c nude mice (male, 4–6 weeks old, weighting 18–20 g) (Shanghai SLAC Laboratory Animal, China) (n = 7/group). Tumor growth was monitored by measuring the length and width of the tumor at the inoculation site. The tumor volume was calculated using the following formula: $V = a \times b^2/2$, where a is the largest diameter and b is the smallest diameter. When the tumor reached 10 mm in length, one mouse in each group was sacrificed, and the subcutaneous tumor was minced into small pieces of equal volume ($1 \times 1 \times 1$ mm^3), which were orthotopically transplanted into the livers in 14 nude mice (n = 7/group). Subsequently, the mice were euthanized, and lung metastasis was assessed at 7 weeks post-tumor implantation. The tumors were fixed in 4% formaldehyde or snap-frozen in liquid nitrogen for further analysis.

Statistical analysis

Statistical analysis was performed using SPSS 25.0 (SPSS, Chicago, IL, USA) and GraphPad Prism8.0 (GraphPad Software, San Diego, CA, USA). Continuous variables are expressed as mean ± standard deviation and analyzed by Student's t test between two groups or one-way analysis of variance for multiple groups. Categorical variables are expressed as absolute number (n) and compared using χ^2 test or Fisher's exact test. OS and RFS between different groups were generated using the Kaplan-Meier method and the log rank test. Cox's proportional hazards regression model was used to analyze independent prognostic factors. A p value of < 0.05 (two-tailed) was considered statistically significant.

Other materials and methods

For more information on other materials and methods, please refer to the supplemental information.

SUPPLEMENTAL INFORMATION

Supplemental information can be found online at https://doi.org/10.1016/j.ymthe.2022.03.015.

ACKNOWLEDGMENTS

We would like to express our sincere gratitude to Prof. Jia Fan and Prof. Jian Zhou for advice and help in the analysis of tissue samples. This work was supported by the National Natural Science Foundation of China (81972715).

AUTHOR CONTRIBUTIONS

R.-X.C., Z.-G.R., and X.-R.Y. participated in the conception and design. R.-X.C. and J.-F.C. designed the experiments and supervised the project. H.-H.L., Y.X., C.-J.L., S.-J.H., X.-H.L., R.Z., Jie Chen, Jun Chen, and D.-M.G. performed the experiments and analyzed the data. R.-X.C. and H.-H.L. wrote the manuscript. All authors contributed in the interpretation of results, manuscript preparation, and revisions. All authors approved the final version to be published.

CONFLICTS OF INTEREST

The authors declare no competing interests.

REFERENCES

1. Sung, H., Ferlay, J., Siegel, R.L., Laversanne, M., Soerjomataram, I., Jemal, A., et al. (2021). Global cancer statistics 2020: GLOBOCAN estimates of incidence and mortality worldwide for 36 cancers in 185 countries. CA Cancer J. Clin. *71*, 209–249.
2. Ishizawa, T., Hasegawa, K., Aoki, T., Takahashi, M., Inoue, Y., Sano, K., et al. (2008). Neither multiple tumors nor portal hypertension are surgical contraindications for hepatocellular carcinoma. Gastroenterology *134*, 1908–1916.
3. Ye, Q.H., Qin, L.X., Forgues, M., He, P., Kim, J.W., Peng, A.C., et al. (2003). Predicting hepatitis B virus-positive metastatic hepatocellular carcinomas using gene expression profiling and supervised machine learning. Nat. Med. *9*, 416–423.
4. Tang, Z.Y., Ye, S.L., Liu, Y.K., Qin, L.X., Sun, H.C., Ye, Q.H., et al. (2004). A decade's studies on metastasis of hepatocellular carcinoma. J. Cancer Res. Clin. Oncol. *130*, 187–196.
5. Affo, S., Yu, L.X., and Schwabe, R.F. (2017). The role of cancer-associated fibroblasts and fibrosis in liver cancer. Annu. Rev. Pathol. *12*, 153–186.
6. Schrader, J., Gordon-Walker, T.T., Aucott, R.L., van Deemter, M., Quaas, A., Walsh, S., et al. (2011). Matrix stiffness modulates proliferation, chemotherapeutic response, and dormancy in hepatocellular carcinoma cells. Hepatology *53*, 1192–1205.
7. Fattet, L., Jung, H.Y., Matsumoto, M.W., Aubol, B.E., Kumar, A., Adams, J.A., et al. (2020). Matrix rigidity controls epithelial-mesenchymal plasticity and tumor metastasis via a mechanoresponsive EPHA2/LYN complex. Dev. Cell *54*, 302–316.e307.
8. Marasco, G., Colecchia, A., Colli, A., Ravaioli, F., Casazza, G., Bacchi Reggiani, M.L., et al. (2019). Role of liver and spleen stiffness in predicting the recurrence of hepatocellular carcinoma after resection. J. Hepatol. *70*, 440–448.
9. Akins, N.S., Nielson, T.C., and Le, H.V. (2018). Inhibition of glycolysis and glutaminolysis: an emerging drug discovery approach to combat cancer. Curr. Top. Med. Chem. *18*, 494–504.
10. Luo, X., Cheng, C., Tan, Z., Li, N., Tang, M., Yang, L., et al. (2017). Emerging roles of lipid metabolism in cancer metastasis. Mol. Cancer *16*, 76.
11. Liu, Q.P., Luo, Q., Deng, B., Ju, Y., and Song, G.B. (2020). Stiffer matrix accelerates migration of hepatocellular carcinoma cells through enhanced aerobic glycolysis via the MAPK-YAP signaling. Cancers (Basel) *12*, 490.
12. Bertero, T., Oldham, W.M., Grasset, E.M., Bourget, I., Boulter, E., Pisano, S., et al. (2019). Tumor-stroma mechanics coordinate amino acid availability to sustain tumor growth and malignancy. Cell Metab. *29*, 124–140.e110.
13. Dong, Y., Zheng, Q., Wang, Z., Lin, X., You, Y., Wu, S., et al. (2019). Higher matrix stiffness as an independent initiator triggers epithelial-mesenchymal transition and facilitates HCC metastasis. J. Hematol. Oncol. *12*, 112.
14. Stowers, R.S., Shcherbina, A., Israeli, J., Gruber, J.J., Chang, J., Nam, S., et al. (2019). Matrix stiffness induces a tumorigenic phenotype in mammary epithelium through changes in chromatin accessibility. Nat. Biomed. Eng. *3*, 1009–1019.
15. Hulver, M.W., Berggren, J.R., Carper, M.J., Miyazaki, M., Ntambi, J.M., Hoffman, E.P., et al. (2005). Elevated stearoyl-CoA desaturase-1 expression in skeletal muscle contributes to abnormal fatty acid partitioning in obese humans. Cell Metab. *2*, 251–261.
16. Levental, K.R., Yu, H., Kass, L., Lakins, J.N., Egeblad, M., Erler, J.T., et al. (2009). Matrix crosslinking forces tumor progression by enhancing integrin signaling. Cell *139*, 891–906.

17. Wei, S.C., Fattet, L., Tsai, J.H., Guo, Y., Pai, V.H., Majeski, H.E., et al. (2015). Matrix stiffness drives epithelial-mesenchymal transition and tumour metastasis through a TWIST1-G3BP2 mechanotransduction pathway. Nat. Cell Biol. *17*, 678–688.

18. Baglieri, J., Brenner, D.A., and Kisseleva, T. (2019). The role of fibrosis and liver-associated fibroblasts in the pathogenesis of hepatocellular carcinoma. Int. J. Mol. Sci. *20*, 1723.

19. Xie, L.T., Gu, J.H., Chai, W.L., Chen, R.D., Zhao, Q.Y., Kong, D.X., et al. (2020). Preoperative detection of liver fibrosis in hepatocellular carcinoma patients using 2D shear wave elastography: where to measure? Ultrasound Med. Biol. *46*, 1412–1423.

20. Masuzaki, R., Tateishi, R., Yoshida, H., Goto, E., Sato, T., Ohki, T., et al. (2009). Prospective risk assessment for hepatocellular carcinoma development in patients with chronic hepatitis C by transient elastography. Hepatology *49*, 1954–1961.

21. Shili-Masmoudi, S., Wong, G.L., Hiriart, J.B., Liu, K., Chermak, F., Shu, S.S., et al. (2020). Liver stiffness measurement predicts long-term survival and complications in non-alcoholic fatty liver disease. Liver Int. *40*, 581–589.

22. Vining, K.H., and Mooney, D.J. (2017). Mechanical forces direct stem cell behaviour in development and regeneration. Nat. Rev. Mol. Cell Biol. *18*, 728–742.

23. Solis, A.G., Bielecki, P., Steach, H.R., Sharma, L., Harman, C.C.D., Yun, S., et al. (2019). Mechanosensation of cyclical force by PIEZO1 is essential for innate immunity. Nature *573*, 69–74.

24. Discher, D.E., Janmey, P., and Wang, Y.L. (2005). Tissue cells feel and respond to the stiffness of their substrate. Science *310*, 1139–1143.

25. Elosegui-Artola, A., Andreu, I., Beedle, A.E.M., Lezamiz, A., Uroz, M., Kosmalska, A.J., et al. (2017). Force triggers YAP nuclear entry by regulating transport across nuclear pores. Cell *171*, 1397–1410.e1314.

26. Provenzano, P.P., and Keely, P.J. (2011). Mechanical signaling through the cytoskeleton regulates cell proliferation by coordinated focal adhesion and Rho GTPase signaling. J. Cell Sci. *124*, 1195–1205.

27. Liu, N., Zhou, M., Zhang, Q., Zhang, T., Tian, T., Ma, Q., et al. (2018). Stiffness regulates the proliferation and osteogenic/odontogenic differentiation of human dental pulp stem cells via the WNT signalling pathway. Cell Prolif. *51*, e12435.

28. Lesage, F., Maingret, F., and Lazdunski, M. (2000). Cloning and expression of human TRAAK, a polyunsaturated fatty acids-activated and mechano-sensitive K(+) channel. FEBS Lett. *471*, 137–140.

29. Thumkeo, D., Watanabe, S., and Narumiya, S. (2013). Physiological roles of Rho and Rho effectors in mammals. Eur. J. Cell Biol. *92*, 303–315.

30. Tzima, E., Irani-Tehrani, M., Kiosses, W.B., Dejana, E., Schultz, D.A., Engelhardt, B., et al. (2005). A mechanosensory complex that mediates the endothelial cell response to fluid shear stress. Nature *437*, 426–431.

31. Hac-Wydro, K., Jedrzejek, K., and Dynarowicz-Łatka, P. (2009). Effect of saturation degree on the interactions between fatty acids and phosphatidylcholines in binary and ternary Langmuir monolayers. Colloids Surf. B Biointerfaces *72*, 101–111.

32. Wang, B., and Tontonoz, P. (2019). Phospholipid remodeling in physiology and disease. Annu. Rev. Physiol. *81*, 165–188.

33. Tiberti, M.L., Antonny, B., and Gautier, R. (2020). The transbilayer distribution of polyunsaturated phospholipids determines their facilitating effect on membrane deformation. Soft Matter *16*, 1722–1730.

34. Urbanelli, L., Buratta, S., Logozzi, M., Mitro, N., Sagini, K., Raimo, R.D., et al. (2020). Lipidomic analysis of cancer cells cultivated at acidic pH reveals phospholipid fatty acids remodelling associated with transcriptional reprogramming. J. Enzyme Inhib. Med. Chem. *35*, 963–973.

35. Miyazaki, M., Bruggink, S.M., and Ntambi, J.M. (2006). Identification of mouse palmitoyl-coenzyme A Delta9-desaturase. J. Lipid Res. *47*, 700–704.

36. Ran, H., Zhu, Y., Deng, R., Zhang, Q., Liu, X., Feng, M., et al. (2018). Stearoyl-CoA desaturase-1 promotes colorectal cancer metastasis in response to glucose by suppressing PTEN. J. Exp. Clin. Cancer Res. *37*, 54.

37. Bai, Y., McCoy, J.G., Levin, E.J., Sobrado, P., Rajashankar, K.R., Fox, B.G., et al. (2015). X-ray structure of a mammalian stearoyl-CoA desaturase. Nature *524*, 252–256.

38. Tracz-Gaszewska, Z., and Dobrzyn, P. (2019). Stearoyl-CoA desaturase 1 as a therapeutic target for the treatment of cancer. Cancers (Basel) *11*, 948.

39. Ng, K.Y., Shea, Q.T., Wong, T.L., Luk, S.T., Tong, M., Lo, C.M., et al. (2021). Chemotherapy-enriched THBS2-deficient cancer stem cells drive hepatocarcinogenesis through matrix softness induced histone H3 modifications. Adv. Sci. (Weinh) *8*, 2002483.

40. Sánchez-Martínez, R., Cruz-Gil, S., Gómez de Cedrón, M., Álvarez-Fernández, M., Vargas, T., Molina, S., et al. (2015). A link between lipid metabolism and epithelial-mesenchymal transition provides a target for colon cancer therapy. Oncotarget *6*, 38719–38736.

41. Lin, L., Ding, Y., Wang, Y., Wang, Z., Yin, X., Yan, G., et al. (2017). Functional lipidomics: palmitic acid impairs hepatocellular carcinoma development by modulating membrane fluidity and glucose metabolism. Hepatology *66*, 432–448.

42. Owen, D.M., Rentero, C., Magenau, A., Abu-Siniyeh, A., and Gaus, K. (2011). Quantitative imaging of membrane lipid order in cells and organisms. Nat. Protoc. *7*, 24–35.

43. Sun, Y.F., Wang, P.X., Cheng, J.W., Gong, Z.J., Huang, A., Zhou, K.Q., et al. (2020). Postoperative circulating tumor cells: an early predictor of extrahepatic metastases in patients with hepatocellular carcinoma undergoing curative surgical resection. Cancer Cytopathol *128*, 733–745.

44. Fenner, J., Stacer, A.C., Winterroth, F., Johnson, T.D., Luker, K.E., and Luker, G.D. (2014). Macroscopic stiffness of breast tumors predicts metastasis. Sci. Rep. *4*, 5512.

45. Zhang, W., Zhu, X.D., Sun, H.C., Xiong, Y.Q., Zhuang, P.Y., Xu, H.X., et al. (2010). Depletion of tumor-associated macrophages enhances the effect of sorafenib in metastatic liver cancer models by antimetastatic and antiangiogenic effects. Clin. Cancer Res. *16*, 3420–3430.

YMTHE, Volume *30*

Supplemental Information

An SCD1-dependent mechanoresponsive pathway promotes HCC invasion and metastasis through lipid metabolic reprogramming

Hua-Hua Liu, Yang Xu, Cao-Jie Li, Shu-Jung Hsu, Xia-Hui Lin, Rui Zhang, Jie Chen, Jun Chen, Dong-Mei Gao, Jie-Feng Cui, Xin-Rong Yang, Zheng-Gang Ren, and Rong-Xin Chen

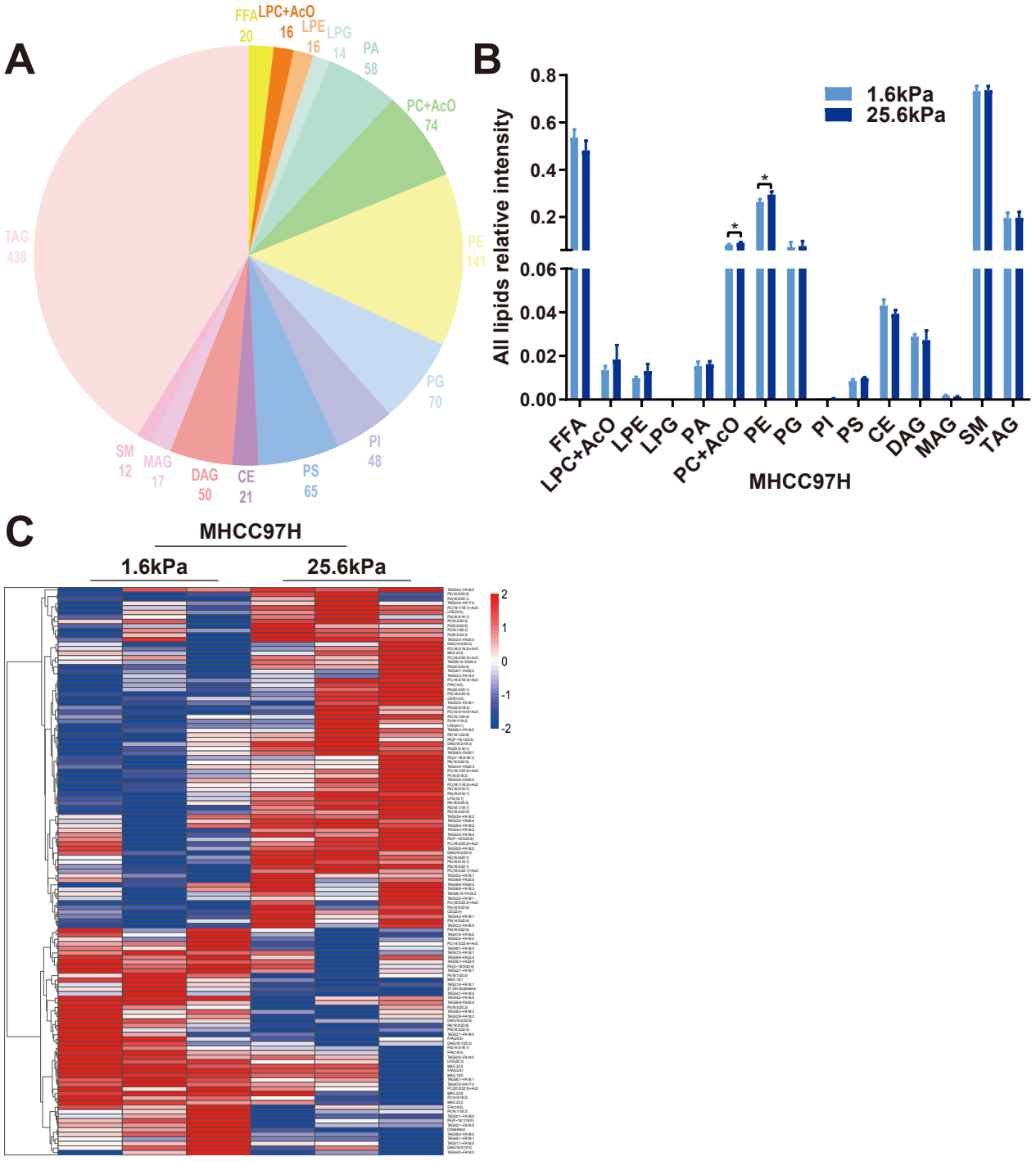

Figure S1. Lipid profiles in HCC cells are altered by matrix stiffness.

(A) Lipid classes were identified in MHCC97H cells cultured on supports at 1.6 kPa or 25.6 kPa in 3D Matrigel overlay culture. (B) Relative intensity of major lipid species in MHCC97H cells on 1.6 kPa or 25.6 kPa support. (C) Lipidomic changes occurring in HCC cells on stiff (25.6 kPa) vs. soft (1.6 kPa) supports were clustered using hierarchical clustering analysis and is shown as a heatmap. Pseudo-colors indicate an increase (red) or a decrease (blue), respectively.

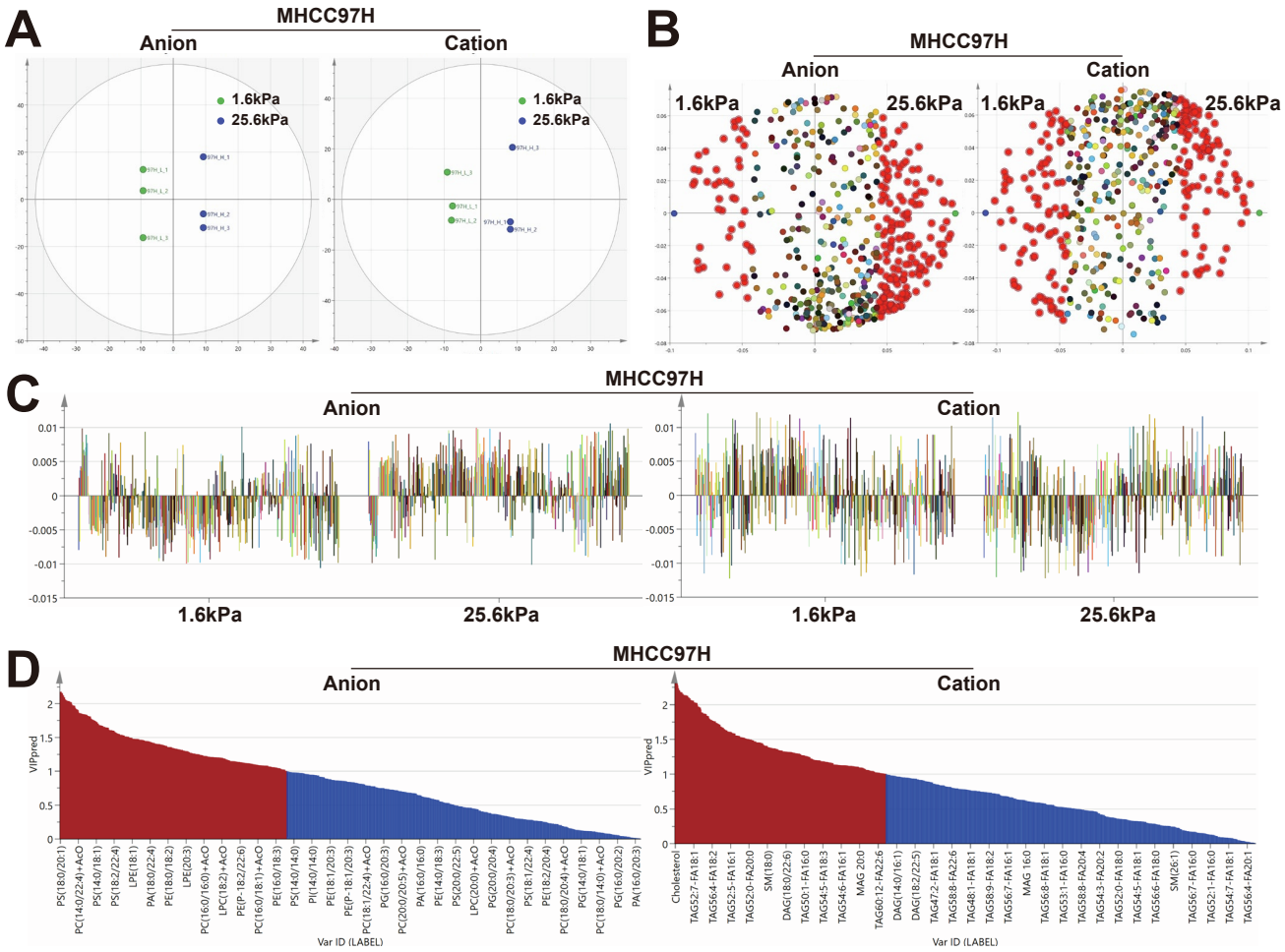

Figure S2. Identification of lipids in HCC cells regulated by matrix stiffness.

(A) Principal component analysis plot for exploratory data of anions and cations in MHCC97H cells on 1.6 kPa or 25.6 kPa support. (B) Lipid molecules in HCC cells on stiff (25.6 kPa) vs. soft (1.6 kPa) support. (C) Distribution of lipids in HCC cells on stiff (25.6 kPa) vs. soft (1.6 kPa) support. (D) Major lipid molecules in HCC cells on stiff (25.6 kPa) vs. soft (1.6 kPa) support were identified by SIMCA software.

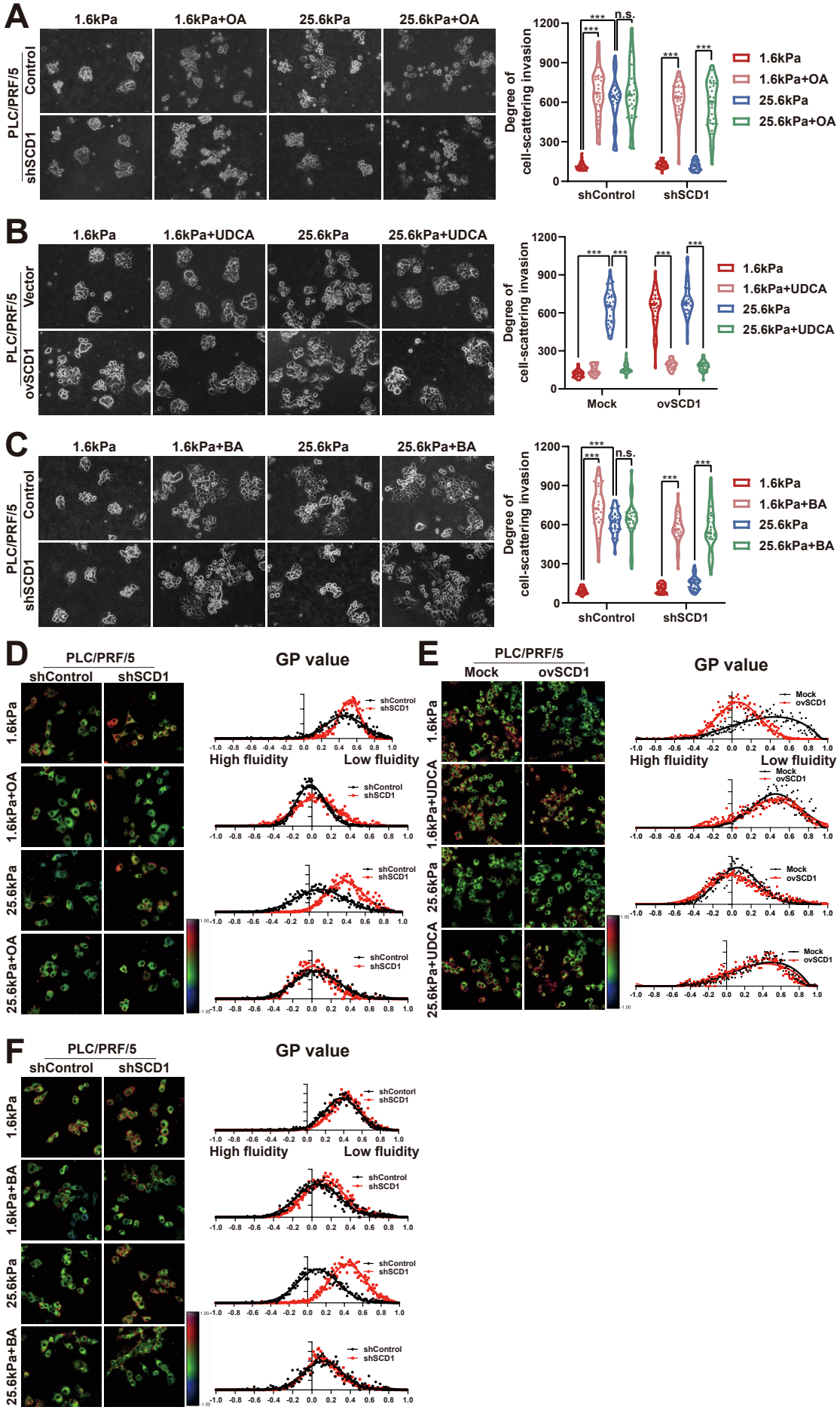
A
1.6kPa
1.6kPa+OA
25.6kPa
25.6kPa+OA
PLC/PRF/5
Control
shSCD1
Degree of cell-scattering invasion
1200
900
600
300
0
***
n.s.
shControl
shSCD1
1.6kPa
1.6kPa+OA
25.6kPa
25.6kPa+OA
B
1.6kPa
1.6kPa+UDCA
25.6kPa
25.6kPa+UDCA
PLC/PRF/5
Vector
ovSCD1
Mock
ovSCD1
1.6kPa
1.6kPa+UDCA
25.6kPa
25.6kPa+UDCA
C
1.6kPa
1.6kPa+BA
25.6kPa
25.6kPa+BA
PLC/PRF/5
Control
shSCD1
shControl
shSCD1
1.6kPa
1.6kPa+BA
25.6kPa
25.6kPa+BA
D
PLC/PRF/5
shControl
shSCD1
GP value
High fluidity
Low fluidity
1.6kPa
1.6kPa+OA
25.6kPa
25.6kPa+OA
E
PLC/PRF/5
Mock
ovSCD1
GP value
High fluidity
Low fluidity
1.6kPa
1.6kPa+UDCA
25.6kPa
25.6kPa+UDCA
F
PLC/PRF/5
shControl
shSCD1
GP value
High fluidity
Low fluidity
1.6kPa
1.6kPa+BA
25.6kPa
25.6kPa+BA

Figure S3. Membrane fluidity mediates matrix stiffness-induced cellular invasion in HCC cells.

(A) PLC/PRF/5 cells expressing control (shControl) or SCD1 shRNA (shSCD1) were cultured on polyacrylamide hydrogels with the indicated rigidities (1.6 kPa and 25.6 kPa) in the presence of OA in 3D Matrigel overlay culture. (B) HCC cells were transfected with Mock or SCD1 expressing plasmid (ovSCD1) and cultured on polyacrylamide hydrogels with the indicated rigidities (1.6 kPa and 25.6 kPa) in 3D Matrigel overlay culture and then treated with membrane-stabilizing agent UDCA. (C) PLC/PRF/5 cells expressing control (shControl) or SCD1 shRNA (shSCD1) were cultured on polyacrylamide hydrogels with the indicated rigidities (1.6 kPa and 25.6 kPa) in 3D Matrigel overlay culture and treated with membrane-agonist compound BA. The in vitro invasion of HCC cells is quantified by the degree of cell scattering using ImageJ software and GraphPad Prism 8. (D) Hue-saturation-brightness images of PLC/PRF/5 cells expressing shControl or shSCD1 in the presence of OA. (E) Hue-saturation-brightness images of PLC/PRF/5 cells transfected with Mock or ovSCD1 treated with/without UDCA. (F) Hue-saturation-brightness images of PLC/PRF/5 cells expressing shControl or shSCD1 treated with/without compound BA. ***, $P < 0.001$.

Table S1. Clinicopathological characteristics of 110 patients with HCC.

Variable		Number of patients (%)
Age(years)	≥50	51(46.4)
	< 50	59(53.6)
Gender	Female	6(5.5)
	Male	104(94.5)
ALT(U/L)	≥40	42(38.2)
	< 40	68(61.8)
Child Pugh	B	1(0.9)
	A	109(99.1)
HBsAg	Yes	101(91.8)
	No	9(8.2)
AFP (ng/ml)	≥400	47(42.7)
	< 400	63(57.3)
Liver Cirrhosis	Yes	84(76.4)
	No	26(23.6)
Encapsulation	Complete	67(60.9)
	Incomplete	43(39.1)
Differentiation	Low	36(32.7)
	High	74(67.3)
Tumor size(cm)	≥5	35(31.8)
	< 5	75(68.2)
Tumor number	Multiple	11(10)
	Single	99(90)
Vascular Invasion	Yes	42(38.2)
	No	68(61.8)
MVI	Yes	42(38.2)
	No	68(61.8)
PVTT	Yes	16(14.5)
	No	94(85.5)
BCLC stage	B+C	19(17.3)
	0+A	91(82.7)
Collagen (%)	≥11.98	55(50)
	< 11.98	55(50)
SCD1	High	58(52.7)
	Low	52(47.3)

Table S2. Univariate and multivariate analysis of factors associated with the RFS in patients with HCC.

	Category	Univariate analysis		Multivariate analysis	
		HR (95% CI)	*P*	HR (95% CI)	*P*
Age(years)	≥50/ < 50	1.212(0.767-1.913)	0.410		
Gender	Male/Female	1.710(0.688-4.250)	0.248		
ALT(U/L)	≥40/ < 40	1.278(0.802-2.036)	0.303		
Child Pugh	B/A	1.102E-07(0-inf)	0.996		
HBsAg	Yes/No	1.292 (0.560-2.979)	0.547		
AFP (ng/ml)	≥400/ < 400	1.472(0.928-2.335)	0.101		
Liver Cirrhosis	Yes/No	1.170(0.672-2.038)	0.579		
Encapsulation	Complete /Incomplete	0.563(0.355-0.895)	0.015	1.017 (0.564-1.836)	0.955
Differentiation	Low/High	1.317(0.812-2.134)	0.264		
Tumor size(cm)	≥5/ < 5	2.369(1.471-3.815)	< 0.001	2.116 (1.259-3.560)	0.005
Tumor number	Single/Multiple	1.005(0.461-2.191)	0.991		
Vascular Invasion	Yes/No	1.871(1.178-2.974)	0.008	0.715(0.090-5.669)	0.751
MVI	Yes/No	1.792(1.129-2.845)	0.013	1.842 (0.236-14.387)	0.560
PVTT	Yes/No	2.469(1.338-4.553)	0.004	1.816 (0.353-9.347)	0.475
BCLC stage	B+C/0+A	2.023 (1.138-3.597)	0.016	0.596(0.138-2.575)	0.488
Collagen (%)	≥11.98/ < 11.98	2.550(1.580-4.116)	< 0.001	0.837(0.482-1.454)	0.527
SCD1	High/Low	2.591(1.588-4.229)	< 0.001	1.583(0.926-2.706)	0.093
Collagen+SCD1	High/Low	8.554(3.879-18.865)	< 0.001	8.947(3.531-22.670)	< 0.001

$P < 0.05$ was regarded as statistically significant and *P* value was calculated by Cox proportional hazards regression.

Table S3. Univariate and multivariate analysis of factors associated with the OS in patients with HCC.

	Category	Univariate analysis		Multivariate analysis	
		HR (95% CI)	*P*	HR (95% CI)	*P*
Age(years)	≥50/ < 50	1.736(0.998-3.017)	0.051	1.904(1.022-3.547)	0.042
Gender	Male/Female	1.873(0.674-5.205)	0.229		
ALT(U/L)	≥40/ < 40	1.254(0.719-2.186)	0.425		
Child-Pugh	B/A	6.754(0.892-51.133)	0.064	17.668(0.789-395.492)	0.070
HBsAg	Yes /No	1.025 (0.370-2.843)	0.962		
AFP (ng/ml)	≥400/ < 400	2.172(1.257-3.754)	0.006	1.631(0.910-2.925)	0.101
Liver cirrhosis	Yes /No	1.270(0.637-2.533)	0.497		
Encapsulation	Complete /Incomplete	0.541(0.314-0.932)	0.027	1.040(0.502-2.153)	0.916
Differentiation	Low/High	1.515(0.866-2.651)	0.145		
Tumor size(cm)	≥5/ < 5	2.214(1.277-3.836)	0.005	2.324(1.274- 4.239)	0.006
Tumor number	Single/Multiple	0.878(0.349-2.207)	0.781		
Vascular invasion	Yes /No	2.160(1.251-3.730)	0.006	6.561(0.820-52.486)	0.076
MVI	Yes /No	1.900(1.098-3.271)	0.022	0.276(0.037-2.075)	0.211
PVTT	Yes /No	1.863(0.934-3.717)	0.078	1.452(0.156-13.504)	0.743
BCLC stage	B+C/ 0+A	1.936 (1.014-3.695)	0.045	0.728(0.094-5.628)	0.761
Collagen (%)	≥11.98/ < 11.98	2.295(1.294-4.070)	0.005	0.492(0.135-1.786)	0.281
SCD1	High/Low	2.562(1.419-4.626)	0.002	1.463(0.709-3.017)	0.303
Collagen+SCD1	High/Low	2.847(1.592-5.092)	< 0.001	5.278(1.396-19.949)	0.014

$P < 0.05$ was regarded as statistically significant and *P* value was calculated by Cox proportional hazards regression.

Supplemental Methods

Cell culture

Human HCC cells MHCC97H (established by Liver Cancer Institute, Zhongshan Hospital of Fudan University, Shanghai, China), PLC/PRF/5, Hep3B and Huh7 (purchased from the cell bank of Chinese Academy of Sciences, Shanghai, China) were grown in Dulbecco's modified Eagle media (Gibco,) supplemented with 10% fetal bovine serum (FBS; Biosun, China) and 1% penicillin-streptomycin (Gibco, USA) at 37°C in a 5% CO_2 incubator. The authenticity of HCC cell lines was validated by DNA Short Tandem Repeat (STR) analysis.

Antibodies and reagents

Primary antibodies, including anti-SCD1 (Santa Cruz, 1:200 for immunostaining, 1,000 for Western blot), anti-α-Tubulin (Beyotime Biotechnology, China; 1:1,000), anti-N-cadherin (CST,1:1,000 for Western blot), anti-E-cadherin (CST, 1:1,000 for Western blot), anti-human laminin (Abcam, 1:200), anti-β1-integrin clone 6S6 (Millipore Sigma, USA; 50 μg/mL), control IgG1 (CST, USA) and anti-Ubiquitin(P4D1) (CST, USA) were used. The secondary antibodies included anti-mouse conjugated with Alexa Fluor 488 (Life Technologies) and anti-mouse conjugated horseradish peroxidase (HRP) antibodies (Beyotime Biotechnology). Focal adhesion kinase (FAK) inhibitor (PF562271, Selleck, China) was solubilized in dimethylsulfoxide (DMSO) and utilized at a concentration of 0.5 μM.

Generation of stable gene knockdown or overexpression cell lines

Stable gene knockdown or overexpression cell lines were generated using lentiviral plasmid vectors (Genechem, China). Briefly, the lentiviruses carrying SCD1 shRNA or control shRNA, carrying SCD1 cDNA or control vector were infected into HCC cells MHCC97H and PLC/PRF/5 with the multiplicity of infection (MOI) of 20 and 10, respectively. SCD1 shRNA1, 5'-CGTCCTTATGACAAGAACATT-3'; SCD1 shRNA2, 5'-CTACGGCTCTTTCTGATCATT-3'; SCD1 shRNA3, 5'-CCCACCTACAAGGATAAGGAA-3'; Control shRNA, 5'-TTCTCCGAACGTGTCACGT-3'. Infected cells were then selected for stable cell subclones with 3-6 μg/mL puromycin. SCD1 protein levels were analyzed by Western blot.

Polyacrylamide hydrogels with variable stiffness

A collagen-coated polyacrylamide hydrogel system with incremental stiffness ranging from 1.6 kilo-Pascal (kPa) to 25.6 kPa was constructed between glass coverslips by mixing acrylamide and bis-acrylamide (Usen, China) at variable ratios, TEMED, and ammonium persulfate (APS, Sigma, USA)

according to the formula described by Dou et al.[1] A 1 mm-thick flat hydrogel was formed and cut into appropriate sizes after polymerization. After rinsing with phosphate-buffered saline (PBS) and sterilizing by microwave heating, the gels were treated with dopamine hydrochloride solution (1 mg/mL in 50 mM HEPES, pH 8.5, Sigma) for 20 min, followed by incubation with collagen I solution (0.06 mg/mL in PBS, pH 7.4) (BD Biosciences, USA) for 60 min and pre-incubation in FBS-free culture medium at 4 °C overnight.

Three-dimensional (3D) cell culture

The 3D cell culture was carried out using the method described previously by Wei et al.[2] Briefly, HCC cells were seeded on the polyacrylamide hydrogels with different stiffness in six-well plates and cultured in 2% Matrigel DMEM supplemented with 10% FBS and 1% penicillin and streptomycin. The media were replaced every 4 days. The formed cell spheres at 10-day post culture were photographed using a contrast-phase Olympus BX51 inverted microscope (200× magnification) under a bright field. The cell spheres protruding into the Matrigel were scored as round, compact morphology or spread, cell-dissociated and invasive phenotype. The degree of cell scattering was defined as a coefficient of variation (percentage) of scattered distribution of cells in each cell sphere, quantified by ImageJ software in 50 cell spheres from five random fields per well, indicating cell invasion.

Reverse transcription and quantitative real-time polymerase chain reaction (qRT-PCR)

Total RNA was extracted from cells using TRIzol reagent (Invitrogen, USA). The cDNA was synthesized from 1 μg RNA using a cDNA Synthesis Super Mix Kit (Yeasen, China) and used as template for a real-time PCR amplification with gene specific primers and FastStart Universal SYBR Green Master (Rox) Kit (Roche, USA) on an Applied Biosystems 7500 PCR system. The expression value of the target gene was calculated using the 2-ΔΔCt method normalized to that of β-actin and expressed as fold-change. The following primers were used for SCD1 amplification: sense primer, 5′-GCCCCTCTACTTGGAAGACGA-3′ and antisense primer, 5'-AAGTGATCCCATACAGGGCTC-3'. The β-actin was amplified using sense primer, 5′-CATGTACGTTGCTATCCAGGC-3' and antisense primer, 5'-CTCCTTAATGTCACGCACGAT-3'.

Western blot

Western blot analysis was performed as described previously.[3,4] Briefly, the protein was extracted from total cells lysates, separated by 10% sodium dodecyl sulfate-polyacrylamide gel electrophoresis (SDS-PAGE), and transferred to polyvinylidene difluoride (PVDF) membrane (Merck Millipore, USA). The

membrane was blocked with 5% fat-free milk and probed with primary antibodies overnight at 4 °C, followed by incubation with horseradish peroxidase (HRP)-conjugated secondary antibody. The reaction was developed by an enhanced chemiluminescence assay. For IP, cell lysates incubated with IP antibodies against SCD1 (1:100, Abcam, USA) rotationally at 4 ℃ overnight. On the second day, Protein A Magnetic Beads (73778, CST) were added for pulling down SCD1 at room temperature for 20 min.

Lipidomic profile analysis

Total lipids were extracted using a modified method by Bligh and Dyer.[5] Briefly, 1×10^6 cells were sonicated for 30 s in 900 μL ddH_2O. Then, the suspension was mixed with 1 mL chloroform (HPLC grade) (Billerica, MA, USA) and 2 mL methanol (Billerica, MA, USA) for 1 min, followed by the addition of 10 μL internal standard cocktails (Alabaster, AL, USA) and 1 mL chloroform for 1 min. Subsequently, 1 mL ddH_2O was added to the mixture before centrifugation at 2000 ×*g*, 4 °C for 15 min. After stratification, the lower layer of chloroform phase was withdrawn into a new glass tube (Kimble, USA), evaporated under nitrogen gas, and reconstituted with 200 μL of dichloromethane: methanol (1:2) containing 10 mM ammonium acetate (Billerica). Of this, 180 uL was transferred into the sample bottle. Finally, lipid samples were subjected to LC-MS analysis as described previously (5). Each experiment was repeated three times.

Lipid compositions were identified by mass spectrometry and compared to internal standards for quantification as reported previously.[6] Under multi-reaction monitoring (MRM) mode, the normal-phase silica liquid chromatography-coupled (NPLC) triple quadrupole mass spectrometer (QTRAP® 6500, SCIEX, USA) was used to extract the lipid for the positive and negative electrospray ionization mode, and Q-Trap was used to scan the precursor/product ion to obtain the chemical structures of the lipids. The peak area of each pair obtained by mass spectrometry was processed and quantified using MultiQuant™ software (AB, SCIEX), and lipidomic data were processed with SIMCA software (v 14.1). The relative signal intensities were calculated by normalization to cell numbers and total signal intensities. The peak changes between samples were compared by manual quantification. Multivariate statistical analysis and cluster analysis were carried out using MetaboAnalyst 4.0 (http://www.metaboanalyst.ca).

Immunofluorescence

Briefly, cells were washed with PBS, fixed with 4% paraformaldehyde (Beyotime Biotechnology), permeabilized with 0.5% TritonX-100 (Beyotime Biotechnology), and blocked with 5% bovine serum albumin at room temperature for 30 min. Then, the samples were incubated with primary antibodies

overnight at 4 ℃, followed by incubation with secondary antibody for 60 min at room temperature and counterstained for nucleus with 4',6-diamidino-2-phenylindole (DAPI, Thermo Fisher, USA). The images were acquired using an Olympus BX51 microscope (200× magnification), and the signals were quantified using ImageJ analysis software (National Institutes of Health, Bethesda, MD, USA).

SCD1 degradation assay

SCD1 protein stability in HCC cells on polyacrylamide gels with different stiffness was analyzed by Western blot in the presence of protein synthesis inhibitor cycloheximide (Selleck, China) at a concentration of 20 μg/mL or cycloheximide with proteasome inhibitor MG-132 (MCE, China) at 10 μM. At each time point, cells were harvested and lysed with RIPA buffer. Equivalent amounts of total protein were analyzed by Western blot.

Immunohistochemistry

The paraffin-embedded tumor tissue sections were deparaffinized with xylene and dehydrated with alcohol. After microwave antigen retrieval and blocking with 5% goat serum, sections were incubated with primary antibodies overnight at 4 ℃ and secondary antibodies at room temperature for 30 min, followed by development with 3,3'-diaminobenzidine (DAB) and counterstaining with hematoxylin. The images were captured under Olympus BX51 microscope (×100 magnification) and analyzed using Image-Pro Plus 6.0 (Media Cybernetics, USA).

Analysis of The Cancer Genome Atlas (TCGA) data

The publicly available data were downloaded from the TCGA Research Network. For the survival analysis, we examined the expression of the SCD1and COL1A1 in TCGA-HCC cohort (368 tumoral samples). The median of all samples was used as the threshold and the tumor samples were splitted into high- and low-expression groups. Kaplan-Meier survival curves were generated and group comparisons were assessed by a log-rank test.

Supplemental References

1. Dou, C., Liu, Z., Tu, K., Zhang, H., Chen, C., Yaqoob, U., et al. (2018). P300 Acetyltransferase Mediates Stiffness-Induced Activation of Hepatic Stellate Cells into Tumor-Promoting Myofibroblasts. Gastroenterology 154, 2209-2221.e2214.

2. Wei, S.C., Fattet, L., Tsai, J.H., Guo, Y., Pai, V.H., Majeski, H.E., et al. (2015). Matrix stiffness drives epithelial-mesenchymal transition and tumour metastasis through a TWIST1-G3BP2 mechanotransduction pathway. Nat Cell Biol 17, 678-688.

3. Zhang, R., Ma, M., Lin, X.H., Liu, H.H., Chen, J., Chen, J., et al. (2018). Extracellular matrix collagen I promotes the tumor progression of residual hepatocellular carcinoma after heat treatment. BMC Cancer 18, 901.

4. Sun, J., Zhou, C., Zhao, Y., Zhang, X., Chen, W., Zhou, Q., et al. (2021). Quiescin sulfhydryl oxidase 1 promotes sorafenib-induced ferroptosis in hepatocellular carcinoma by driving EGFR endosomal trafficking and inhibiting NRF2 activation. Redox Biol 41, 101942.

5. Bligh, E.G., and Dyer, W.J. (1959). A rapid method of total lipid extraction and purification. Can J Biochem Physiol 37, 911-917.

6. Gao, D., Zhang, L., Song, D., Lv, J., Wang, L., Zhou, S., et al. (2019). Values of integration between lipidomics and clinical phenomes in patients with acute lung infection, pulmonary embolism, or acute exacerbation of chronic pulmonary diseases: a preliminary study. J Transl Med 17, 162.